Towards a high-resolution sea ice model: exploring the potential of modelling ice floe fracture with the peridynamic method

Yuan Zhang, Wenjun Lu, Raed Lubbad, Sveinung Løset, Andrei Tsarau and Knut Vilhelm Høyland

Department of Civil and Environmental Engineering, Faculty of Engineering, Norwegian University of Science and Technology, 7491, Trondheim, Norway

Abstract

Sea ice deformation is concentrated at Linear Kinematic Features (LKFs) such as ridges and leads. Ridging and leads opening processes are highly related to sea ice fracture. Different rheology models have been successfully applied in various scenarios. However, most of the approaches adopted are based on continuum mechanics that do not explicitly model fracture processes. There are emerging needs for a more physically informed modelling methods that explicitly address fracture at the kilometre scale. In pursuing this objective, we explored in this paper the potential of applying a promising mesh free numerical method, peridynamics (PD), in modelling ice floe (~km) fractures. PD offers a physically and mathematically consistent theory through which spontaneous emergence and propagation of cracks can be achieved. The integral nature of the governing equations in PD remains valid even if a crack appears. We numerically investigated in this paper the tensile fracture (e.g., lead opening) of an elastic heterogenous ice floe. The modelling results were compared with published numerical results obtained by another numerical method. The potentials and challenges of PD in this application are discussed and summarized.

Keywords: Ice floe; fracture; peridynamics; lead opening

1. Introduction

Sea ice fracture is a significant and important natural phenomenon with broad-ranging implications for safety, navigation, climate research, ecology, infrastructure, resource extraction, search and rescue operations, and scientific exploration in polar and icy regions (Bamber and others, 2022, Ingels and others, 2021). The processes of ridging and opening of leads are closely linked to sea ice fracture. Sea ice fracture results in swift ocean-air thermal exchanges and the generation of new ice. More specifically, leads in the Arctic Ocean contribute to approximately 25-40% of the overall ice production in the region (Kwok, 2006). Enhancing our understanding and modelling capabilities of the fracture of sea ice at global level is of utmost importance.

Various ice rheology models (Feltham, 2008), including those for simulating ice deformation at meso- and large-scales (mesoscale refers to 50–500 km and large scale beyond that), have been proposed. Most are based on the Viscous Plastic (VP) model by Hibler (1979) and the Elastic-Viscous-Plastic (EVP) model by Hunke and Dukowicz (1997). However, recent research suggests that while the VP model accurately captures global sea ice motion, it lacks finer-scale deformation properties crucial for operational modelling (Girard and others, 2009). This underscores the need for alternative models, such as the Elasto-Brittle (EB) model implemented by Girard et al. (2011), forming the foundation for the neXtSIM model. Yet, the EB model has limitations in long-term fracture process depiction. Dansereau et al. (2016) introduced the Maxwell-EB (MEB) model, which integrates the Mohr-Coulomb theory and shows promise in long-term simulations. Additionally, continuum mechanics approaches, like anisotropic ice rheology (Wilchinsky and Feltham, 2012), address sea ice fractures but often rely on ad-hoc assumptions to simplify modelling.

2

As reviewed above, most approaches used in sea ice deformation modelling rely on continuum mechanics, where ice fracture is not explicitly considered. Throughout history, fracture mechanics concepts have not been extensively utilized to address ice fracturing. This is largely due to the inherent complexity of fracture mechanics, especially when compared to the simplified nature of strength theory. Unlike fracture mechanics, strength theory lacks fracture-related scaling laws and tends to be conservative at large scales when using the same local-scale (0.1–10 m) material parameters (Lu, 2022). Another factor contributing to the lack of explicit consideration of ice fracture is the significant computational costs associated with the accurate modelling of this complex phenomenon. Nonetheless, we believe fracture plays a crucial role in influencing ice dynamics across various scales, particularly at local scales. However, our understanding of its effects remains limited at present. As the length scale of block being fractured exceeds tens of meters, the application of fracture mechanics analysis becomes imperative. This is because strength theory proves inadequate in characterizing physical processes that happen over a range of different sizes (spatial scale) and time durations (temporal scale) (Lu and others, 2022). Given the modelling gap and importance of ice fracture, this paper explores possibilities in explicitly simulating ice fractures at large scales.

Various numerical methods have been developed to explicitly model sea ice fractures, primarily at local scales. These methods can be broadly categorized as mesh-based and particle-based approaches. Mesh-based methods, such as conventional nonlinear finite element method involving element erosion (Liu and Amdahl, 2010, Lu and others, 2012) or nodes splitting (Herrnring and Ehlers, 2021), continuum damage model (Kolari, 2007, Kolari, 2017), extended Finite Element Method (XFEM) (Lu and others, 2018, Xu and others, 2020), cohesive element method (CEM) (Lu and others, 2014b, Feng and others, 2016) and cohesive surface model (Kuutti and others, 2013) harness the advantage of traditional FEM with fracture mechanic theories. However, they require additional criteria to characterize complex crack propagation

3

behaviours like turning, branching, and arresting; and eventual fragmentations. These methods often require complex crack tracking algorithms and topology representation. Particle-based methods, such as smooth particle hydrodynamics (SPH) (Marquis and others, 2022, Shen and others, 2000), discrete element method (DEM) (Damsgaard and others, 2018, Herman, 2016, Hopkins and Thorndike, 2006, van den Berg, 2019, van den Berg and others, 2018, Lu and others, 2012, Prasanna and others, 2022) and lattice method (van den Berg, 2016, Slepyan and others, 1999, Jirásek and Bažant, 1995), discretize equations of continuum media using a specific volume, taking advantage of their meshfree characteristics. This feature makes them particularly well-suited for simulating fracture scenarios characterized by significant deformations. Despite their inherent advantage of handling discontinuity/fracture, these methods are rather computationally demanding. This is largely due to the often-simplified particle-particle interaction formulations. Without sufficient number of particles (e.g., around a running crack tip), it becomes demanding to characterize the complicated force and displacement field around crack tips. Another innovative approach is the use of Phase Field Damage Models (PFMs), which employ Griffith's theory to study the elastic failure and simulate crack propagation through a potential energy minimization process (Wu and others, 2020, Omatuku, 2019). PFMs was applied in studying the failure of a heterogeneous ice floe using an elastic constitutive model (Dinh and others, 2023) and ice shelves using a viscoelastic constitutive model (Sondershaus and Müller, 2022). These studies demonstrate the potential of PFMs and their possible future applications in high-resolution ice fracture modelling. This method, however, has been shown to be very computationally expensive which overshadows its large-scale applications.

The current paper aims to investigate floe-scale sea ice fracture using another novel computational method called peridynamics (PD). PD is a non-local approach that shows promise in modelling various materials, structures, and systems. It offers an alternative to

4

traditional continuum mechanics, which relies on local concepts such as stress and strain. PD has several advantages, including the ability to model discontinuities like cracks without the need for complex meshing techniques or crack tracking algorithms. It is effective in predicting large deformations and material failures, which can be challenging in traditional continuum mechanics. Recent developments in PD theory have been successfully applied to localized sea ice fracture Vazic (2020) and its interaction with structures (Zhang and others, 2022, Zhang and others, 2021(a), Zhang and others, 2023a, Zhang and others, 2023b).

To the best of our knowledge, the present study demonstrates the first attempt to apply the PD theory in simulating large-scale ice fracture. Our objective is to explore the suitability and scalability of this particle-based method for high-resolution (~ m) ice fracture simulations at large scales,

In this work, we focus on the tensile fracture of an ice floe. We begin by validating our PD model and studying key PD parameters, including particle spacing and horizon size, through a benchmark case (Section 3). The benchmark case entails a simplified tensile failure setup involving linear elastic and homogeneous ice material, where analytical solutions are available. To further explore the capabilities of PD and align our results with existing publications, we simulate tensile fractures of a heterogenous ice floe with uneven thicknesses (Section 4). Through comparisons and discussions, we expose the potential and challenges of the PD method in this application (Section 5).

2. Description of the PD method

2.1 Peridynamic model for elastic sea ice

Peridynamics (PD) is a non-local formulation of continuum mechanics that is oriented toward deformations with discontinuities, especially fractures. Unlike spatial derivatives common in classic continuum mechanics (e.g., the concept of stress and strain), PD employs integral operators to represent these phenomena. The discretization of the domain in PD

5

involves particles that interact with their neighbouring particles within a specific distance known as the horizon (H_x). Figure 1 provides a visual representation of the fundamental principle of PD theory, where Particle i at position $\mathbf{x}$ [m] interacts with Particle j at position $\mathbf{x}'$ [m]. Under the influence of external forces, the particle i experiences displacement $\mathbf{u}$ [m] while the particle j undergoes displacement $\mathbf{u}'$ [m]. Consequently, this deformation induces a force state term $\mathbf{t}$, which has a unit of [N/m^6] acting on the particle i and another force state term $\mathbf{t}'$ [N/m^6] acting on the particle j. In PD theory, the equation of motion for a material point is defined in Eq. (1) (Madenci and Oterkus, 2014). The previously introduced 'force state' terms $\mathbf{t}$ and $\mathbf{t}'$, after a volume integration, yield a concept of force density [N/m^3] on both sides of Eq. (1).

$$\rho(\mathbf{x})\ddot{\mathbf{u}}(\mathbf{x}, t) = \int_{H_x} (\mathbf{t}(\mathbf{u}' - \mathbf{u}, \mathbf{x}' - \mathbf{x}, t) - \mathbf{t}'(\mathbf{u} - \mathbf{u}', \mathbf{x} - \mathbf{x}', t)) dV' + \mathbf{b}(\mathbf{x}, t), \tag{1}$$

In Eq. (1), $\rho(\mathbf{x})$ [kg/m^3] represents the density of the sea ice, $\ddot{\mathbf{u}}(\mathbf{x}, t)$ [m/s^2] represents the acceleration of the discretized ice particle, and $\mathbf{b}(\mathbf{x}, t)$ [N/m^3] is a body force. In the present work, the fracture problem of two-dimensional ice floes is studied, and the Poisson's ratio of sea ice equals to 0.33. Consequently, we employ the bond-based PD equation rather than the general state-based PD for numerical simulation. The rationale behind this choice lies in the fact that the force density vectors $\mathbf{t}$ and $\mathbf{t}'$ in the bond-based PD are equal in magnitude and parallel to the relative position vector. Under this assumption, the Poisson's ratio (ν) is fixed at 1/3 for 2D simulations, which suits our requirements for simulating sea ice. In contrast, in the general state-based PD, the force density vector is unconstrained, allowing for the free setting of Poisson's ratio. However, state-based PD is computationally expensive.

The expression of the force state $\mathbf{t}$ [N/m^6] for an elastic and isotropic ice material in Eq. (1) is:

$$\mathbf{t} = -\mathbf{t}' = 2\delta s b \frac{\mathbf{y}' - \mathbf{y}}{|\mathbf{y}' - \mathbf{y}|} \, . \tag{2}$$

In the above formula, b represents a parameter of PD (presented in Eq. (4)), δ [m] represents the size of the horizon (H_x). $\mathbf{y}$ [m] and $\mathbf{y}'$ [m] are the position vectors of particle i and particle j after deformation, respectively. Generally, the shape of the horizon is a circular shape in 2D (disk). Therefore, horizon size δ refers to the radius of a disk, as shown in Figure 1. s is a unitless scalar, called the bond stretch, representing the deformation between two particles (see Eq. (3)). The relation between bond stretch and the 'force state' in Eq. (2) demonstrates the constitutive model of linear elastic ice material.

$$s = \frac{|\mathbf{y}' - \mathbf{y}| - |\mathbf{x}' - \mathbf{x}|}{|\mathbf{x}' - \mathbf{x}|} \, . \tag{3}$$

b [Pa/m^5] is a scaler related to a bond constant c [Pa/m^4] which usually is expressed by ice properties (elastic modulus, E [Pa]), and horizon size δ [m]. The relations are:

$$b = \frac{c}{4\delta} \quad \text{with} \quad c = \frac{9E}{\pi h \delta^3} \quad \text{for 2D with } \upsilon = \frac{1}{3} \, , \tag{4}$$

where h [m] is the thickness of the ice floe.

Figure 1. near here.

2.2 Material failure model

In PD theory, material failure simulation can be viewed at two levels (see Figure 2). The first level is the particle-particle interaction elimination through a binary damage function (i.e., 0 or 1). For example, in the 'crack initiation phase' in Figure 2, for particle $i = 1$, its bonds 1-11 and 1-12 are assigned a value of 0 and are thus eliminated. The failure at this level does not necessarily entail a complete failure for a material point (e.g., for particle i=1 in Figure 2, there are still 10 particles remaining connected to it). The second level failure reminiscent a domain damage concept, in which, a percentage of particle-particle interactions within the horizon of a material point are eliminated. This percentage (from 0 to 1) is termed as a damage variable

7

and is a continuous function represents the level of 'damage', with '1' representing the complete break-off of a material point (e.g., see the total elimination of particle $i = 1$ in the last phase of Figure 2). Any other value in between 0-1 gives us the possibility to characterize the location of a macroscopic crack, e.g., with a damage variable of 0.5 (e.g., see the crack formation phase in Figure 2), it represents a crack cutting through the material point, whose 50% particle-particle connections in the horizon have been eliminated.

Figure 2. near here

Mathematically, the above damaging processes are achieved through the introduction of two additional functions. At the first level failure, particle-particle interaction can be eliminated through the concept of bond rupture. Bond rupture can be determined using a variety of failure criteria. We choose to use the critical stretch criterion. It is a straightforward and widely used criterion to predict material failure; and is particularly derived for tensile failures. This criterion involves comparing the stretch s (in Eq. (3)) between two material particles with a critical value, which is called the critical stretch (s_C).

$$\Omega(t, \mathbf{x}' - \mathbf{x}) = \begin{cases} 1, & s < s_C, \quad \text{unbroken or visible bond} \\ 0, & s \geq s_C, \quad \text{broken or invisible bond} \end{cases}. \tag{5}$$

A binary failure function $\Omega(t, \mathbf{x}' - \mathbf{x})$ is introduced in accordance with the critical stretch criterion in Eq. (5). This function is incorporated in Eq. (1) to characterize material failure in Eq. (6) as (Silling and Askari, 2005, Madenci and others, 2022)

$$\rho(\mathbf{x})\ddot{\mathbf{u}}(\mathbf{x}, t) = \int_{H_x} (\mathbf{t}(\mathbf{u}' - \mathbf{u}, \mathbf{x}' - \mathbf{x}, t) - \mathbf{t}'(\mathbf{u} - \mathbf{u}', \mathbf{x} - \mathbf{x}', t))\Omega(t, \mathbf{x}' - \mathbf{x})dV' + \mathbf{b}(\mathbf{x}, t). \tag{6}$$

$\Omega(t, \mathbf{x}' - \mathbf{x})$ defines the magnitude of an irreversible failure, thereby changing the load distribution within the body and allowing crack initiation and propagation. With this criterion, crack propagation occurs spontaneously without requiring a predefined direction.

In Eq. (5), the unitless critical stretch s_C is derived from the critical energy release rate G_c [N/m]. The 2D bond-based version of s_C is expressed as (Madenci and others, 2022)

$$s_C = \sqrt{\frac{\pi G_c}{3K_{2D}\delta}} ,$$ (7)

in which K_{2D} [Pa] is bulk modulus in 2D.

Failure function in Eq. (5) only defines the interaction elimination between two particles. In the second level, the determination of crack initiation and propagation involves the introduction of a PD damage variable (denoted as $\varphi(\mathbf{x},t)$, see Figure 2), which integrates all the failure function in the horizon of particle of interest. Therefore, $\varphi(\mathbf{x},t)$ is simply a weight ratio between the broken bonds and the total number of initial bonds connecting a material particle within the horizon. At crack initiation, a particle engages in interactions with all ice particles within its horizon, resulting in a local damage variable equalling to 0 (i.e., no damage or no crack initiation). On the other hand, the formation of a crack surface leads to the elimination of half of the interactions within the horizon, yielding a local damage variable equalling to 0.5. The damage variable is presented in Eq. (8).

$$\varphi(\mathbf{x},t) = 1 - \frac{\int_{H_x} \Omega(t, \mathbf{x}' - \mathbf{x})dV'}{\int_{H_x} dV'} .$$ (8)

2.3 Discretization and solvers

Our approach primarily relies on the open-source PD software Peridigm (Littlewood and others, 2023). We also utilize a finite element mesh generator to construct a hexahedral mesh of the ice domain, which is then saved as an external file for PD model construction purposes. As mentioned before, the 2D bond-based explicit PD solver is employed. This solver evaluates the force states (denoted as $\mathbf{t}$ and $\mathbf{t}'$) in Eq. (1) at each time step and applies them to each bond

9

in the discrete model. The time steps are determined based on the criterion in Bobaru and others (2016), that is

$$\Delta t_{critical} = \sqrt{\frac{2\rho}{\sum_p \Delta V_p \frac{18K_{2D}}{(\mathbf{x}' - \mathbf{x})\pi\delta^4}}} , \tag{9}$$

in which ρ is the density, p iterates over all the neighbours of the given material point, ΔV_p is the volume associated with neighbours p. Then, we utilize Paraview for post-processing.

3. Benchmark case: Splitting of an Edge Cracked Rectangular Plate (ECRP)

In this section, a benchmark test of our numerical implementation is carried out on a simplified Mode I splitting failure of an ECRP. Extensive studies on this tensile fracture setup have been carried out both theoretically (Bhat, 1988, Bhat and others, 1991, Dempsey and Zhao, 1993, Mulmule and Dempsey, 1997, Lu and others, 2015c) and experimentally (Adamson and Dempsey, 1998, Adamson and others, 1995, Dempsey and others, 1999b, Dempsey and others, 1999a, Lu and others, 2015a).

Among all the available theories, we build our validation case against the existing analytical solution of the Mode I splitting of an ECRP. We choose the simplest Linear Elastic Fracture Mechanics solutions (available from Lu and others (2015b)) as our benchmark case. The solution is general to any type of linear elastic material. However, while building our PD numerical model, we chose parameters following the experiments of Dempsey and others (1999a), See Table 1. Please note the Mode-I fracture energy is set to match that in Lu and others (2014a) for comparison purpose.

3.1 Model setup

Figure 3 illustrates the model setup, in which each mesh element represents a spatial volume occupied by PD particle. The solution of the governing equation (Eq. (6)) is obtained by performing a volume integral over all hexahedron volumes in the horizon. To compare with existing analytical solutions, the ECRP is modelled as homogeneous, isotropic and linear

10

elastic in the PD model. This ice plate is also assumed to fail brittlely, where LEFM can be applied. However, it should be noted that PD is not limited to these idealizations Zhang and others, 2021(b).

Table 1. near here

Figure 3. near here

Following the approach in the study conducted by Vazic and others (2020), a constant particle body force is assumed as the loading condition in the current study and is applied to the three particles in the volume they occupy along the pre-crack, as shown in Figure. 3. The magnitude of this constant load is expected to be small (to minimize dynamic effects), yet large enough to propagate the central crack. In post processing, we extract the splitting force F_y for comparison with analytical solutions. Since we have performed a load-controlled simulation here, we took an unconventional but equivalent approach to extract the splitting force. In detail, we integrate bond-bond forces along the remaining ligament of the central crack. This gives us the 'fracture resistance' in force term. In this way, we manage to extract the splitting force F_y, which is in equilibrium of the 'fracture resistance'.

The particle spacing (dx) and the horizon size (δ) are critical factors influencing the computational process, establishing the optimal values for these parameters is crucial to obtain accurate results. Before directly presenting the results and comparison, a series of convergence studies (δ-convergence and dx-convergence) are performed in the following.

3.2 Convergence analysis

The δ-convergence and dx-convergence are first studied to determine the optimal parameters for the current PD simulations. We choose dx as 0.1 m, 0.15 m, 0.2 m, 0.3 m, 0.5 m for the dx-convergence study. The horizon size is $\delta = mdx$, where m denotes a multiplier factor. We chose $\delta = mdx = (2.015, 3.015, 4.015)dx$ for the δ-convergence study. Discretization and critical stretches calculated by Eq. (7) are shown in Table 2.

11

Table 2. near here

Convergence study results are presented in **Error! Reference source not found.**a and **Error! Reference source not found.**b. In these figures, we presented the normalized splitting force ($F_y / (hK_{IC}L^{1/2})$, in which $K_{IC} = \sqrt{EG_c}$ represents fracture toughness of sea ice versus the normalized crack length (A/L). Simulation outputs from PD are generated in the time domain. Normalized splitting force versus normalized crack length in **Error! Reference source not found.** are constructed by synchronizing the simulated force and crack length history.

Figure 4(a). near here

Figure 5(b). near here

Based on **Error! Reference source not found.**a, it can be observed that varying particle spacings has minimal impact on the splitting force value., All curves reach their maximum value when A/L is between 0.14 and 0.19. However, as the particle spacing increases, the oscillation amplitude of the splitting force also increases. Notably, when the particle distances are set at 0.1 m and 0.15 m, the vibration amplitude of the dimensionless splitting force is the smallest, and all curves converge at around these values. Consequently, a particle distance of 0.15 m is chosen as the optimal setting for accuracy considerations.

δ-convergence analysis plays a crucial role in determining the appropriate horizon size, which greatly affects the simulation results. As depicted in **Error! Reference source not found.**b, it is evident that the results are in close agreement when the multiplier factors m for the horizon size are set to 3.015 and 4.015. Notably, the multiplier factor of 3.015 is widely used in various other research fields (Madenci and Oterkus, 2014), further affirming its reliability.

The convergence results are encouraging. Especially, it has revealed an optimal setting, i.e., m=3.015 and dx=0.15 m for our benchmark test (to be discussed in Section 5.1).

12

3.3 Simulation results of the splitting of ECRP

Fixing the multiplier factor m=3.015 and dx=0.15 m, the simulated results of crack path for ice tensile failure are depicted in Figure 6. The central edge crack propagates straight ahead, as theoretically expected.

Figure 6. near here

Then, the normalized splitting force of PD simulation is compared with analytical solution found in Lu and others (2014a), numerical result obtained by Lu and others (2015c), and FEM result obtained by Bhat (1988), as shown in Figure 7.

Figure 7. near here

The normalized splitting force initially increases and then decreases as the normalized crack length increases, reaching a peak when the normalized crack length is between 0.14 and 0.2. This trend is consistent with the results from the compression of an edge-cracked rectangular plate conducted by Hallam and others (1989). Moreover, We compare the calculated results with those calculated by other methods for the same case. The results depicted in Figure 7 indicate that the calculated values for the ice plate's splitting force from the 2D Bond Based PD exhibit a reasonably satisfactory agreement with those methods. Further discussions will be presented in Section 5.2. Next, we will explore PD's capability in a more realistic tensile fracture scenario, i.e., multiple fracturing of a heterogeneous ice floe.

4. Numerical experiment on the fracture of a heterogeneous ice floe

Currently, detailed experimental results to validate the fracture and crack propagation at the floe scale are scarce. Therefore, we performed a comparative study against a numerical experiment carried out by Dinh and others (2023). In our study, we employed the same sea ice model, boundary conditions, and physical parameters as Dinh and others (2023). The only divergence lies in the choice of modelling approach: they utilized the phase field model (PFM), whereas we employed our proposed PD model.

In their work, ice floes are simply modelled as a linear elastic body. What has been implied in their simplified linear elastic treatment is the assumption that many nonlinear features of sea ice, e.g., material weakening and creep behaviour, can be introduced by the presence of pre-existing 'cracks'/weak zones. i.e., as long as these weak zones are explicitly modelled, a simplified material model (e.g., linear elastic) is good enough to characterize the overall nonlinear behaviour of the heterogeneous ice floe. These pre-existing 'cracks'/weak zones are modelled through the introduction of ice thickness variations at different zones. Fracture of sea ice is modelled according to the Griffith theory, i.e., LEFM. All these features are in accordance with our current PD model development.

4.1 Model setup

Following the work of Dinh and others (2023), we built a same square ice floe (1 km in length and 1 m in thickness) in the PD discretization domain (see **Error! Reference source not found.**). All the input parameters for simulation are listed in Table 3. A prescribed boundary condition with a displacement of 5 mm is applied on the left edge of ice floe. The right edge is fixed (see **Error! Reference source not found.**a). Note that the boundary conditions are imposed by three layers of fictional boundary particles as required by PD theory. These layers consist of particles that occupy a volume of space and have the same parameters as other particles in the ice body. However, these particles are not within the actual geometry of the ice and are added additionally, as shown in Figure. 7(a).

Varying ice thickness values are assigned to different zones matching those of literature (Dinh and others, 2023). Two ice floes are modelled in this study (see **Error! Reference source not found.**b and **Error! Reference source not found.**c). Corresponding ice thickness information is presented in Table 4.

Table 3. near here

Figure 8(a). near here

14

Figure 9(b). near here

Figure 10(c). near here

Table 4. near here

4.2 Simulation results on the fracture of a heterogeneous ice floe

Error! Reference source not found. illustrates the displacement contour and damage variable contour (i.e., φ value in Eq. (8)) computed using the PD method, as well as the displacement and damage result obtained by Dinh and others (2023) through PFM modelling.

Figure 11(a-1). near here

Figure 12(a-2). near here

Figure 13(a-3). near here

Figure 14(b-1). near here

Figure 15(b-2). near here

Figure 16(b-3). near here

As **Error! Reference source not found.** demonstrates, our simulated crack paths agree well with the results from PFM: 1) both ice floes were fractured into two pieces. 2) The cracks predominantly initiate from weak zones (i.e., thin ice) and propagate in parallel to the boundary, aligning with any existing defects. The area of non-zero motion in Figure 8(b-1) appears because this area is almost completely separated from the rest of the ice plate. Only a small portion of the particles in this area interact with its horizon particles, which are located inside the more intact part of the ice body. Consequently, the velocity and displacement of particles in this area are subject to minimal constraints, leading to rapid changes in speed and displacement during numerical calculations. Please also note that positive displacement is to the right and negative displacement is to the left. As you can see, there is a white area without a damage value in Figure 8(b-1) and (b-2). This is because zero thickness is represented by an absence of material, which is why there is no damage value in this gap area.

15

Additionally, PD simulates crack branches (as shown in case 1, **Error! Reference source not found.**(b-2)). Even no additional complete fragmentations are formed, PD reflects the location of potential cracks about to occur through the damage variable (Eq. (7)), which can be observed in **Error! Reference source not found.**(b-2). In this scenario, a damage value equal to or greater than 0.5 is designated as indicative of a clear crack path. Conversely, when the damage falls below 0.5, it signifies a weakened area that may serve as a potential site for crack propagation. These demonstrate an advantage of PD in solving failure problems.

5. Discussion

In this paper, we evaluated the potential of a promising numerical method, the PD method, in simulating ice fracture at large scale. As a starting point, tensile fracture is the focus. In Section 3, we presented simulation results of a benchmark case (i.e., the splitting of an ECRP), and performed relevant parametric studies. In Section 4, we presented results on a comparative study on the fracture modelling of a heterogeneous ice floe. In this section, we discuss our results in the following aspects:

5.1 PD versus classic fracture modelling/analysis

Figure 7 presents comparisons of different methods in simulating the splitting of an ECRP. In general, PD agrees well with the other classic fracture modelling (i.e., FEM) and analytical solution approaches. This signifies PD theory's capabilities and the correctness of our modelling in this benchmark test. This also offers some insights in comparing different approaches. Naturally, analytical solutions for a fracture problem, in which the presence of a pre-existing crack is needed, are primarily used in idealized scenarios. In this case, it is the idealized geometry (i.e., a rectangular geometry with a central edge crack) and material properties (i.e., a homogeneous, isotropic and linear elastic material). PD's modelling capabilities, as well as other numerical approaches, are evidently beyond these idealizations yet offers reasonably accurate results. Classic numerical approaches (e.g., FEM used by Bhat

16

(1988) and Lu and others (2015c)) focuses on calculating the stress intensity factors (SIFs) at the crack tip with continuous model updating procedures. This means that FEM modelling and calculations must be repeated every time a new crack position is required, with each crack position resulting from an independent static problem solution. Consequently, FEM does not predict the spontaneous and dynamic expansion of cracks. Each data point in the FEM results shown in Figure 6 corresponds to an individual simulation. In contrast, PD, as its name indicates, is a dynamic analysis in the time domain. The PD results in Figure 7 were obtained in one single simulation run, thus alleviating us from supplying new information in deciding crack propagation and generating crack conforming new meshes.

5.2 On the accuracy of PD in simulating ice fracture

In our benchmark test and its related parametric studies, we see how PD simulations results behaves with varying particle spacings and horizon size (**Error! Reference source not found.**); and how the results compare with analytical solutions (Figure 6).

First, we discuss the oscillatory nature of our PD simulations. Figure 2 illustrates that the breakup of bonds leads to the formation of cracks. Bond rupture is a discrete process. These bonds do not break simultaneously. Each bond's rupture led to either weakening (easy to understand) or strengthening (potentially due to the generation of a favourable bond-bond interaction to resist fracture) of the cracked geometry. This leads to the oscillation in splitting force.

Then, the difference between the analytical solution and PD simulation results are further examined. We analyse the differences arise primarily from the following two sources:

- Difficulties in locating the crack tip

Results presented in **Error! Reference source not found.** and Figure 6 require knowledge of crack length A, or the location of the crack tip. This is not straightforward in PD modelling. As introduced in Section 2.2, material failure (at the crack tip) is modelled by a continuous

17

function ($\varphi(\mathbf{x},t)$). It is therefore difficult to clearly pinpoint the location of a crack tip, leading to difficulties in defining the exact crack length A. To specify an exact location of the crack tip (also the crack length), we define the midpoint between the particles whose $\varphi(\mathbf{x},t) \geq 0.35$ and the next particle whose $\varphi(\mathbf{x},t) < 0.35$ as the crack tip. As shown in Figure 9, the crack length should be $A = \dfrac{y_4 + y_3}{2}$. This arbitrary choice may have contributed to the discrepancy between our PD and non-PD solutions. However, in practical applications at large scale, we do not consider this a major drawback. We expect such small deviation will not dramatically alter the fracture pattern at large scales (as is evident in the results in Section 4).

Figure 17. near here

- Displacement control versus load control

In our benchmark test, we applied a constant load at the crack mouth of the ECRP. The splitting of an ECRP is largely a 'softening' process, i.e., the fracture resistance decreases as the crack extends. This is evident from Figure 6, where the normalized splitting force (or fracture resistance) decreases after A/L reaches 0.14. Given the constant loading at the crack mouth, it leads to crack instability (or magnified dynamic effects as crack propagates). On the other hand, analytical solutions were obtained at static equilibrium of each crack length. Normally, to achieve a stable crack growth, a displacement-controlled loading condition would be preferred. Nevertheless, despite the differences in loading condition, the results do not differ significantly. Our primary application of PD involves external loading, such as wind and current acting as surface loads, and floe-floe contact serving as boundary forces. Therefore, we are satisfied with the current load-controlled benchmark test.

5.3 On the inherent efficiency of PD in simulating ice fracture

18

For any numerical method, there is a trade-off between accuracy and efficiency. This trade-off is largely reflected by the spatial (e.g., mesh size and particle spacing) and temporal (i.e., time step) resolution of discretization. Here we discuss the inherent efficiency of PD method.

- Spatial resolution

For PD simulations, there are two important numerical length scales. These are the particle spacing dx and the horizon size δ. These two numbers are correlated through a multiplying factor m. δ-convergence and dx-convergence study results were presented in **Error! Reference source not found.**. This reveals an optimal combination of m=3.015 and dx=0.15 m for our benchmark test. However, a particle spacing of 0.15 m would be quite computationally prohibitive for ~ km-scale of applications. In this regard, further sensitivity studies on PD particle spacing and horizon size are carried out in the fracture of heterogenous ice floe here with more reasonable particle spacing size (i.e., ~ m). The discretization information for the different particle spacing is reviewed in Table 5.

Table 5. near here

Figure 18(a). near here

Figure 19(b). near here

Figure 20(c). near here

Based on the calculation results (see Figure 10), It is evident that different particle distributions and particle spacing in the reasonable range have negligible effects on the crack propagation path, although the cracks exhibit different degrees of fracture. This finding suggests the possibility of utilizing larger PD particle spacings for large scale ice floe fractures simulations.

- Temporal resolution

In the PD method, the prediction of crack propagation relies on explicit solvers to simulate the dynamic growth process and path of the cracks. The numerical stability required for this

19

process imposes strict constraints on the time step, which is considerably smaller than the maximum time step defined by the Courant-Friedrichs-Lewy (CFL) criterion used in the Finite Element Method (FEM) scheme. This characteristic presents a significant challenge when addressing larger time scales and high-resolution scenarios in sea ice fracture problems. We can potentially increase PD's simulation efficiency by employing the implicit integral method for solving or adjust our mesh size making a reasonable trade-off between efficiency and accuracy in this application. Still, we believe these improvements are just superficial numerical improvements. Perhaps the more pressing task at present is to enhance the computational efficiency of PD to facilitate its application to large-scale sea ice damage problems, and potentially integrate it with existing ice rheology models.

5.4 On PD's application in large scale ice fracture simulations

Section 4 shows the PD's capability in simulating the failure of a heterogeneous ice floe at large scale (1 km). The comparison was made against the PFM. At present, only qualitative comparison is made in **Error! Reference source not found.**, which show resemblance between both simulation results. Our intention is not to compare these two methods as there exist many literatures on this issue (e.g., Diehl and others (2022)). Instead, we explore the potential of PD in simulating ice floe fracture at large scale in a same setting. Nevertheless, a visual comparison presented **Error! Reference source not found.**b demonstrates a unique advantage of PD in simulating progressive fragmentation process over the PFM. However, this comes with a cost. Both PD and PFM are computationally expensive.

Computational cost is detrimental for these methods' large-scale applications. One potential solution to apply PD to large-scale sea ice simulations efficiently is to couple PD with a mature and efficient existing model (such as Discrete Element Method, FEM). In this approach, PD solves the domain that includes the fracture, while the rest of the domain is solved by that mature and efficient existing model. We have experience supporting this idea; we have

20

implemented ice fracture simulation in a Discrete Element Method (DEM)-based simulation environment in a selective manner. Specifically, not all ice bodies are simulated for fracture; only those prone to fracture are evaluated (Lubbad and others, 2022). This approach has significantly increased simulation efficiency.

6. Conclusions

The fracture of large-scale sea ice has a great impact on the climate, environment, and Arctic engineering. The research on large-scale sea ice fracture is mostly based on continuum mechanics and lacks physically informed parameterization towards high resolution fracture models. To explore the potential method in modelling explicit sea ice fracture, the present study employed a fracture mechanics featured method, PD theory, to investigate sea ice fracture. As an initial step, we focus on the tensile fracture of a single ice floe. We performed two studies:

1) the splitting of an edge cracked rectangular ice plate (ECRP) and 2) the fracture of a heterogeneous ice floe.

The following conclusions can be drawn from the experimental ice floe fracture simulation and the preceding discussions:

1) PD can reasonably capture the initiation, propagation, branching and bridging of multiple cracks in a heterogeneous ice floe.

2) For the application of PD in simulation ice floe fracture at 1 km, PD's simulation results seem to be minimally affected by particle spacing (up to $\sim$ 6 m). This shows the potential of using PD to achieve high-resolution ($\sim$ m) yet large-scale ($\sim$ km) ice fracture simulations.

3) On temporal scales, the explicit solver used in the current PD method required demandingly small simulation time steps (same but more specific conclusions can also be found in Littlewood and others (2023). This issue may be addressed through

21

established numerical methods, e.g., using an implicit solver. However, this 'superficial' numerical improvement may not be enough for long-term fracture simulations.

4) Similar to other numerical methods (e.g., PFM), PD is computationally demanding. This is considered as one of the major challenges in its large-scale applications. To address this, we need to reconsider the way how we use PD in an ice dynamic model (e.g., DEM) to address large scale ice fractures.

7. Future thinking

We cannot assert with absolute certainty that the PD method is completely superior to other methods, such as PFM or FEM, in predicting large-scale sea ice fracture. Each method has its own advantages and disadvantages. Compared to other methods, PD has higher computational costs, and as the computational volume increases, the costs rise faster than with other methods.

However, the PD method has unique advantages in predicting the initiation and propagation of cracks. Thanks to its self-embedded fracture mathematical model, it can predict the generation and spontaneous expansion of cracks, which significantly contributes to predicting the formation of new ice blocks after large-scale sea ice breakage. We also have the opportunity to further develop PD constitutive models and efficient numerical calculations suitable for large-scale sea ice, achieving accurate results step by step to reach the ultimate goal.

Moreover, it can be found that the present study employed PD to simulate the tensile damage of sea ice, neglecting compression damage. However, compression damage is a significant aspect of sea ice failure. Therefore, it is a subject the authors intend to investigate in the future. Given that compression failure in sea ice typically involves shearing, a literature review suggests that the Mohr-Coulomb criterion could more accurately capture the failure behaviour of large-scale sea ice. Consequently, the authors will incorporate the Mohr-Coulomb model to explore the potential of studying large-scale compression damage by PD simulations.

.

22

Acknowledgements

REFERENCES

Adamson, R.M., J. Dempsey, S.J. DeFranco and Y. Xie 1995. Large-scale in-situ ice fracture experiments: Part I - Experimental aspects. 107-128. https://www.researchgate.net/publication/303813673_Large-scale_in-situ_ice_fracture_experiments_Part_I_-_Experimental_aspects

Adamson, R.M. and J.P. Dempsey 1998. Field-scale in-situ compliance of arctic first-year sea ice. *Journal of Cold Regions Engineering*, **12**(2): 52-63. doi:10.1061/(ASCE)0887-381X(1998)12:2(52)

Bamber, J.L., M. Oppenheimer, R.E. Kopp, W.P. Aspinall and R.M. Cooke 2022. Ice Sheet and Climate Processes Driving the Uncertainty in Projections of Future Sea Level Rise: Findings From a Structured Expert Judgement Approach. Earth's Future, 10(10): e2022EF002772. doi:10.1029/2022EF002772

Bhat, S., S. Choi, T. Wierzbicki and D. Karr 1991. Failure analysis of impacting ice floes. doi:10.1115/1.2919914

Bhat, S.U. 1988. Analysis for splitting of ice floes during summer impact. *Cold Regions Science and Technology*, **15**(1): 53-63. doi:10.1016/0165-232X(88)90038-9

Bobaru, F., J.T. Foster, P.H. Geubelle and S.A. Silling 2016. *Handbook of Peridynamic Modeling*. CRC Press. doi:10.1201/9781315373331

Damsgaard, A., A. Adcroft and O. Sergienko 2018. Application of Discrete Element Methods to Approximate Sea Ice Dynamics. *Journal of Advances in Modeling Earth Systems*, **10**(9): 2228-2244. doi:10.1029/2018ms001299

Dansereau, V., J. Weiss, P. Saramito and P. Lattes 2016. A Maxwell elasto-brittle rheology for sea ice modelling. *The Cryosphere*, **10**(3): 1339-1359. doi:10.5194/tc-10-1339-2016

Dempsey, J.P., R.M. Adamson and S.V. Mulmule 1999a. Scale effects on the in-situ tensile strength and fracture of ice. Part II: First-year sea ice at Resolute, N.W.T. *International Journal of Fracture*, **95**(1): 347-366. doi:10.1023/A:1018650303385

Dempsey, J.P., S.J. Defranco, R.M. Adamson and S.V. Mulmule 1999b. Scale effects on the in-situ tensile strength and fracture of ice Part I: Large grained freshwater ice at Spray Lakes Reservoir, Alberta. *International Journal of Fracture*, **95**(1): 325-345. doi:10.1023/A:1018629107713

Dempsey, J.P. and Z.G. Zhao 1993. Elastohydrodynamic response of an ice sheet to forced sub-surface uplift. *Journal of the Mechanics and Physics of Solids*, **41**(3): 487-506. doi:10.1016/0022-5096(93)90045-H

Diehl, P., R. Lipton, T. Wick and M. Tyagi 2022. A comparative review of peridynamics and phase-field models for engineering fracture mechanics. *Computational Mechanics*, **69**(6): 1259-1293. doi:10.1007/s00466-022-02147-0

Dinh, H., D. Giannakis, J. Slawinska and G. Stadler 2023. Phase-field models of floe fracture in sea ice. *The Cryosphere*, **17**(9): 3883-3893. doi:10.5194/tc-17-3883-2023

Feltham, D.L. 2008. Sea Ice Rheology. *Annual Review of Fluid Mechanics*, **40**(1): 91-112. doi:10.1146/annurev.fluid.40.111406.102151

Feng, D., S.D. Pang and J. Zhang 2016. Parameter Sensitivity in Numerical Modelling of Ice-Structure Interaction With Cohesive Element Method. *ASME 2016 35th International Conference on Ocean, Offshore and Arctic Engineering*. doi:10.1115/omae2016-54687

Girard, L., S. Bouillon, J. Weiss, D. Amitrano, T. Fichefet and V. Legat 2011. A new modeling framework for sea-ice mechanics based on elasto-brittle rheology. *Annals of Glaciology*, **52**(57): 123-132. doi:10.3189/172756411795931499

Girard, L., J. Weiss, J.M. Molines, B. Barnier and S. Bouillon 2009. Evaluation of high-resolution sea ice models on the basis of statistical and scaling properties of Arctic sea ice drift and deformation. Journal of Geophysical Research: Oceans, 114(C8). doi: 10.1029/2008JC005182

Hallam, S. D., Jones, N., and Howard, M. W. 1989: The Effect of Sub-Surface Irregularities on the Strength of Multi-Year Ice, Journal of Offshore Mechanics and Arctic Engineering, 111, 350-353. doi: 10.1115/1.3257106

Herman, A. 2016. Discrete-Element bonded-particle Sea Ice model DESIgn, version 1.3a – model description and implementation. *Geoscientific Model Development*, **9**(3): 1219-1241. doi: 10.5194/gmd-9-1219-2016

Herrnring, H. and S. Ehlers 2021. A Finite Element Model for Compressive Ice Loads Based on a Mohr-Coulomb Material and the Node Splitting Technique. *Journal of Offshore Mechanics and Arctic Engineering*, **144**(2). doi:10.1115/1.4052746

Hibler, W.D. 1979. A Dynamic Thermodynamic Sea Ice Model. *Journal of Physical Oceanography*, **9**(4): 815-846. doi:10.1175/1520-0485(1979)009<0815:Adtsim>2.0.Co;2

Hopkins, M.A. and A.S. Thorndike 2006. Floe formation in Arctic sea ice. *Journal of Geophysical Research*, **111**(C11). doi:10.1029/2005jc003352

Hunke, E.C. and J.K. Dukowicz 1997. An elastic–viscous–plastic model for sea ice dynamics. *Journal of Physical Oceanography*, **27**(9): 1849-1867. doi:10.1175/1520-0485(1997)027<1849:AEVPMF>2.0.CO;2

Ingels, J., R.B. Aronson, C.R. Smith, A. Baco, H.M. Bik, J.A. Blake, A. Brandt, M. Cape, D. Demaster, E. Dolan, E. Domack, S. Fire, H. Geisz, M. Gigliotti, H. Griffiths, K.M. Halanych, C. Havermans, F. Huettmann, S. Ishman, S.A. Kranz, A. Leventer, A.R. Mahon, J. McClintock, M.L. McCormick, B.G. Mitchell, A.E. Murray, L. Peck, A. Rogers, B. Shoplock, K.E. Smith, B. Steffel, M.R. Stukel, A.K. Sweetman, M. Taylor, A.R. Thurber, M. Truffer, A. van de Putte, A. Vanreusel and M.A. Zamora-Duran 2021. Antarctic ecosystem responses following ice-shelf collapse and iceberg calving: Science review and future research. WIREs Climate Change, 12(1): e682. doi: 10.1002/wcc.682

Jirásek, M. and Z.P. Bažant 1995. Particle Model for Quasibrittle Fracture and Application to Sea Ice. *Journal of Engineering Mechanics*, **121**(9): 1016-1025. doi:10.1061/(ASCE)0733-9399(1995)121:9(1016)

Kolari, K. 2007. Damage mechanics model for brittle failure of transversely isotropic solids: Finite element implementation. https://publications.vtt.fi/pdf/publications/2007/P628.pdf

Kolari, K. 2017. A complete three-dimensional continuum model of wing-crack growth in granular brittle solids. *International Journal of Solids and Structures*, **115-116**: 27-42. doi:10.1016/j.ijsolstr.2017.02.012

Kuutti, J., K. Kolari and P. Marjavaara 2013. Simulation of ice crushing experiments with cohesive surface methodology. *Cold Regions Science and Technology*, **92**: 17-28. doi:10.1016/j.coldregions.2013.03.008

Kwok, R. 2006. Contrasts in sea ice deformation and production in the Arctic seasonal and perennial ice zones. *Journal of Geophysical Research: Oceans*, **111**(C11). doi:10.1029/2005JC003246

Littlewood, D. J., Shelton, T., & Thomas, J. D. (2013). Estimation of the Critical Time Step for Peridynamic Models (No. SAND2013-5738C). Sandia National Lab.(SNL-NM), Albuquerque, NM (United States).

Littlewood, D.J., M.L. Parks, J.T. Foster, J.A. Mitchell and P. Diehl 2023. The Peridigm Meshfree Peridynamics Code. *Journal of Peridynamics and Nonlocal Modeling*. doi:10.1007/s42102-023-00100-0

Liu, Z. and J. Amdahl 2010. A new formulation of the impact mechanics of ship collisions and its application to a ship–iceberg collision. *Marine Structures*, **23**(3): 360-384. doi:10.1016/j.marstruc.2010.05.003

Lu, W. 2022. Ice Fracture. Springer, Cham, 75-100. (IUTAM Symposium on Physics and Mechanics of Sea Ice). doi:10.1007/978-3-030-80439-8_5

Lu, W., H.-M. Heyn, R. Lubbad and S. Løset 2018. A large scale simulation of floe-ice fractures and validation against full-scale scenario. *International Journal of Naval Architecture and Ocean Engineering*, **10**(3): 393-402. doi:10.1016/j.ijnaoe.2018.02.006

Lu, W., S. Løset, A. Shestov and R. Lubbad 2015a. Design of a field test for measuring the fracture toughness of sea ice. *Proceedings of the International Conference on Port and Ocean Engineering Under Arctic Conditions*. http://www.poac.com/Papers/2015/pdf/poac15Final00251.pdf

Lu, W., R. Lubbad, K. Høyland and S. Løset 2014a. Physical model and theoretical model study of level ice and wide sloping structure interactions. *Cold Regions Science and Technology*, **101**: 40-72. doi:10.1016/j.coldregions.2014.01.007

Lu, W., R. Lubbad and S. Løset 2014b. Simulating Ice-Sloping Structure Interactions With the Cohesive Element Method. *Journal of Offshore Mechanics and Arctic Engineering*, **136**(3). doi:10.1115/1.4026959

Lu, W., R. Lubbad and S. Løset 2015b. In-plane fracture of an ice floe: A theoretical study on the splitting failure mode. *Cold Regions Science and Technology*, **110**: 77-101. doi:10.1016/j.coldregions.2014.11.007

Lu, W., R. Lubbad and S. Løset 2015c. Out-of-plane failure of an ice floe: Radial-crack-initiation-controlled fracture. *Cold Regions Science and Technology*, **119**: 183-203. doi:10.1016/j.coldregions.2015.08.009

Lu, W., R. Lubbad, S. Løset and K.V. Høyland 2012. Cohesive zone method based simulations of ice wedge bending: a comparative study of element erosion, CEM, DEM and XFEM. *21st IAHR International Symposium on Ice*, Dalian, China, 920-938. https://www.iahr.org/library/infor?pid=27128

Lubbad, R., S. Løset, M. van den Berg, W. Lu and S. Govinda 2022. Physics-Based Modelling of Ice Actions and Action Effects on Marine Structures. In Tuhkuri, J. and A. Polojärvi, *eds. IUTAM Symposium on Physics and Mechanics of Sea Ice*, Cham, Springer International Publishing, 275-299. https://link.springer.com/chapter/10.1007/978-3-030-80439-8_14

Madenci, E. and E. Oterkus 2014. *Peridynamic Theory and Its Applications*. doi:10.1007/978-1-4614-8465-3

Madenci, E., P. Roy and D. Behera 2022. *Advances in Peridynamics*. Springer Cham. doi:10.1007/978-3-030-97858-7

Marquis, O., B. Tremblay, J.-F. Lemieux and M. Islam 2022. Smoothed Particle Hydrodynamics Implementation of the Standard Viscous-Plastic Sea-Ice Model and Validation in Simple Idealized Experiments. *The Cryosphere Discussions. [preprint],*. doi:10.5194/tc-2022-163

Mulmule, S.V. and J.P. Dempsey 1997. A Viscoelastic Fictitious Crack Model for the Fracture of Sea Ice. *Mechanics of Time-Dependent Materials*, **1**(4): 331-356. doi:10.1023/A:1008063516422

Omatuku, E.N. 2019. Phase field modeling of dynamic brittle fracture at finite strains. Faculty of Engineering and the Built Environment.) http://hdl.handle.net/11427/30172

Prasanna, M., A. Polojärvi, M. Wei and J. Åström 2022. Modeling ice block failure within drift ice and ice rubble. *Physical Review E*, **105**(4): 045001. doi:10.1103/PhysRevE.105.045001

Shen, H.T., J. Su and L. Liu 2000. SPH Simulation of River Ice Dynamics. *Journal of Computational Physics*, **165**(2): 752-770. doi:10.1006/jcph.2000.6639

Silling, S.A. and E. Askari 2005. A meshfree method based on the peridynamic model of solid mechanics. *Comput Struct*, **83**(17-18): 1526-1535. doi:10.1016/j.compstruc.2004.11.026

Slepyan, L.I., M.V. Ayzenberg-Stepanenko and J.P. Dempsey 1999. A Lattice Model for Viscoelastic Fracture. *Mechanics of Time-Dependent Materials*, **3**(2): 159-203. doi:10.1023/A:1009846932233

Sondershaus, R.S. and R.M. Müller 2022. Phase field model for simulating fracture of ice. *ECCOMAS Congress 2022-8th European Congress on Computational Methods in Applied Sciences and Engineering*. https://www.scipedia.com/public/Sondershaus_Muller_2022a

van den Berg, M. 2016. A 3-D Random Lattice Model of Sea Ice. *Arctic Technology Conference*. doi:10.4043/27335-ms

van den Berg, M. 2019. Discrete numerical modelling of the interaction between broken ice fields and structures. http://hdl.handle.net/11250/2630787

van den Berg, M., R. Lubbad and S. Løset 2018. An implicit time-stepping scheme and an improved contact model for ice-structure interaction simulations. *Cold Regions Science and Technology*, **155**: 193-213. doi:10.1016/j.coldregions.2018.07.001

Vazic, B. 2020. Multi-scale modelling of ice-structure interactions. (Doctor of Philosophy University of Strathclyde.) doi:10.48730/g0pc-ap61

25

Vazic, B., E. Oterkus and S. Oterkus 2020. In-Plane and Out-of Plane Failure of an Ice Sheet using Peridynamics. *Journal of Mechanics*, **36**(2): 265-271. doi:10.1017/jmech.2019.65

Wilchinsky, A.V. and D.L. Feltham 2012. Rheology of Discrete Failure Regimes of Anisotropic Sea Ice. *Journal of Physical Oceanography*, **42**(7): 1065-1082. doi:10.1175/JPO-D-11-0178.1

Wu, J.-Y., V.P. Nguyen, C.T. Nguyen, D. Sutula, S. Sinaie and S.P. Bordas 2020. Phase-field modeling of fracture. *Advances in applied mechanics*, **53**: 1-183. doi:10.1016/bs.aams.2019.08.001

Xu, Y., P. Kujala, Z. Hu, F. Li and G. Chen 2020. Numerical simulation of level ice impact on landing craft bow considering the transverse isotropy of Baltic Sea ice based on XFEM. *Marine Structures*, **71**. doi:10.1016/j.marstruc.2020.102735

Zhang, Y., L. Tao, C. Wang and S. Sun 2022. Peridynamic analysis of ice fragmentation under explosive loading on varied fracture toughness of ice with fully coupled thermomechanics. *Journal of Fluids and Structures*, **112**: 103594. doi:10.1016/j.jfluidstructs.2022.103594

Zhang, Y., L. Tao, C. Wang, L. Ye and S. Sun 2021(a). Numerical study of icebreaking process with two different bow shapes based on developed particle method in parallel scheme. *Applied Ocean Research*, **114**: 102777. doi:10.1016/j.apor.2021.102777

Zhang, Y., L. Tao, L. Ye, C. Wang, S. Sun and W. Lu 2023a. An updated fast continuous contact detection algorithm and its implementation in case study of ice-structure interaction by peridynamics. *Marine Structure*, **89**. doi:10.1016/j.marstruc.2023.103406

Zhang, Y., L. Tao, , C. Wang, L. Ye, and C. Guo 2021(b): Numerical study on dynamic icebreaking process of an icebreaker by ordinary state-based peridynamics and continuous contact detection algorithm, *Ocean Engineering*, 233,. doi: 10.1016/j.oceaneng.2021.109148

Zhang, Y., G. Zhang, L. Tao, C. Wang, L. Ye, S. Sun and K. Han 2023b. Study and Discussion on Computational Efficiency of Ice-Structure Interaction by Peridynamic. *Journal of Marine Science and Engineering*, **11**(6): 1154. doi:10.3390/jmse11061154

List of figure captions
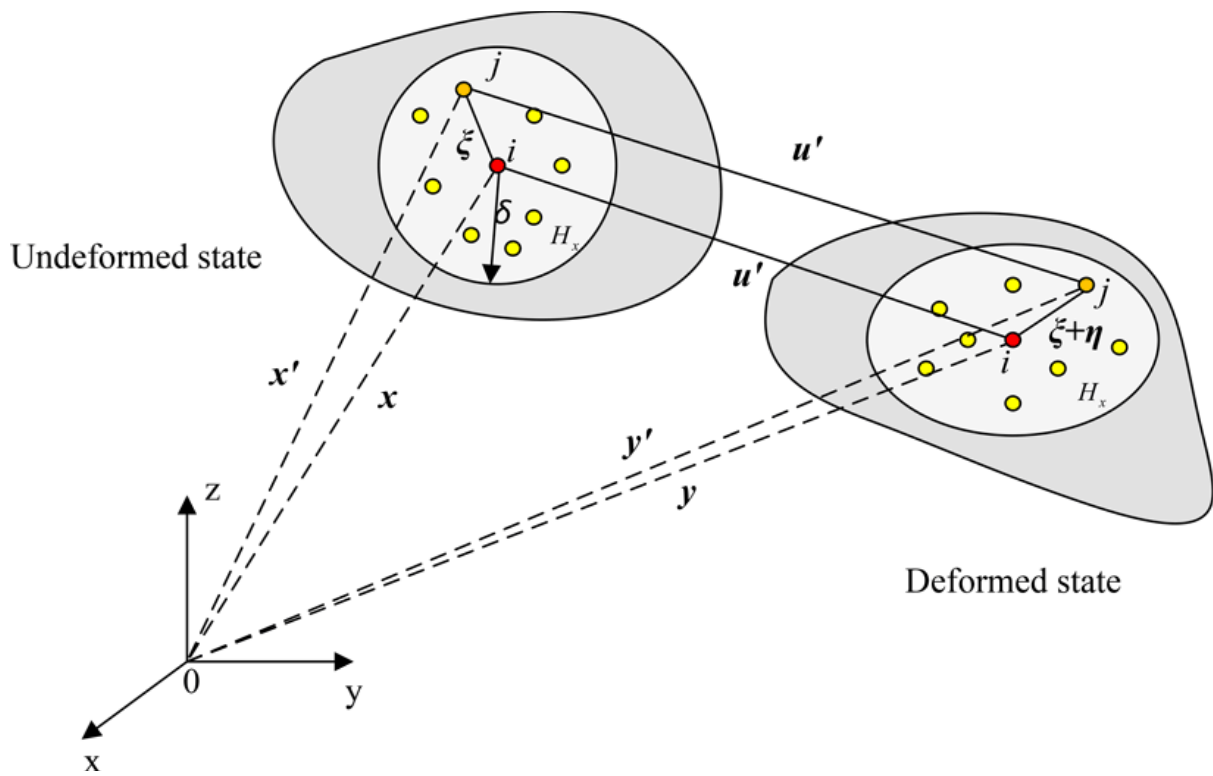
Figure 1. Discretization and particle interactions in PD theory (Zhang and others, 2021).
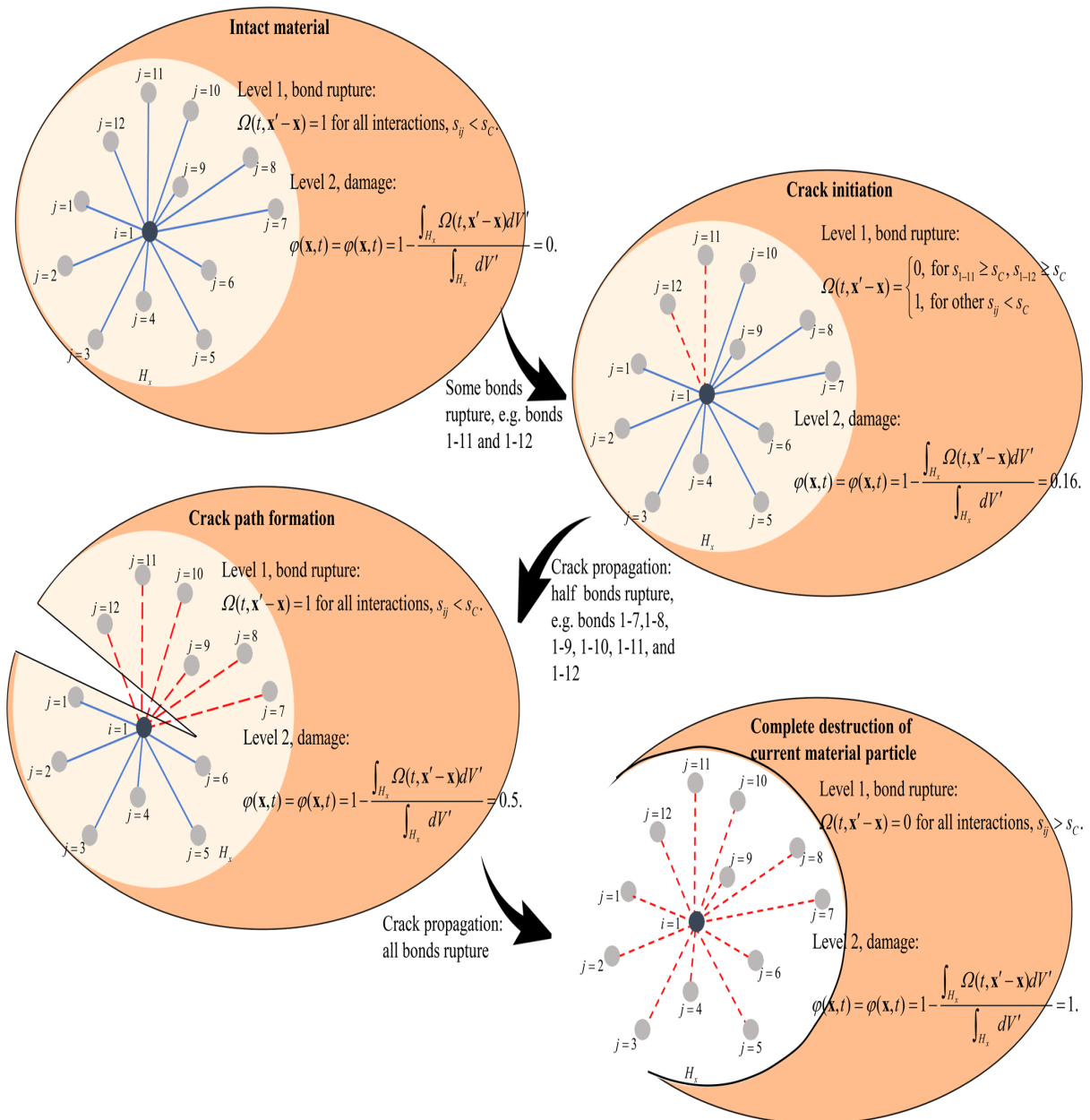
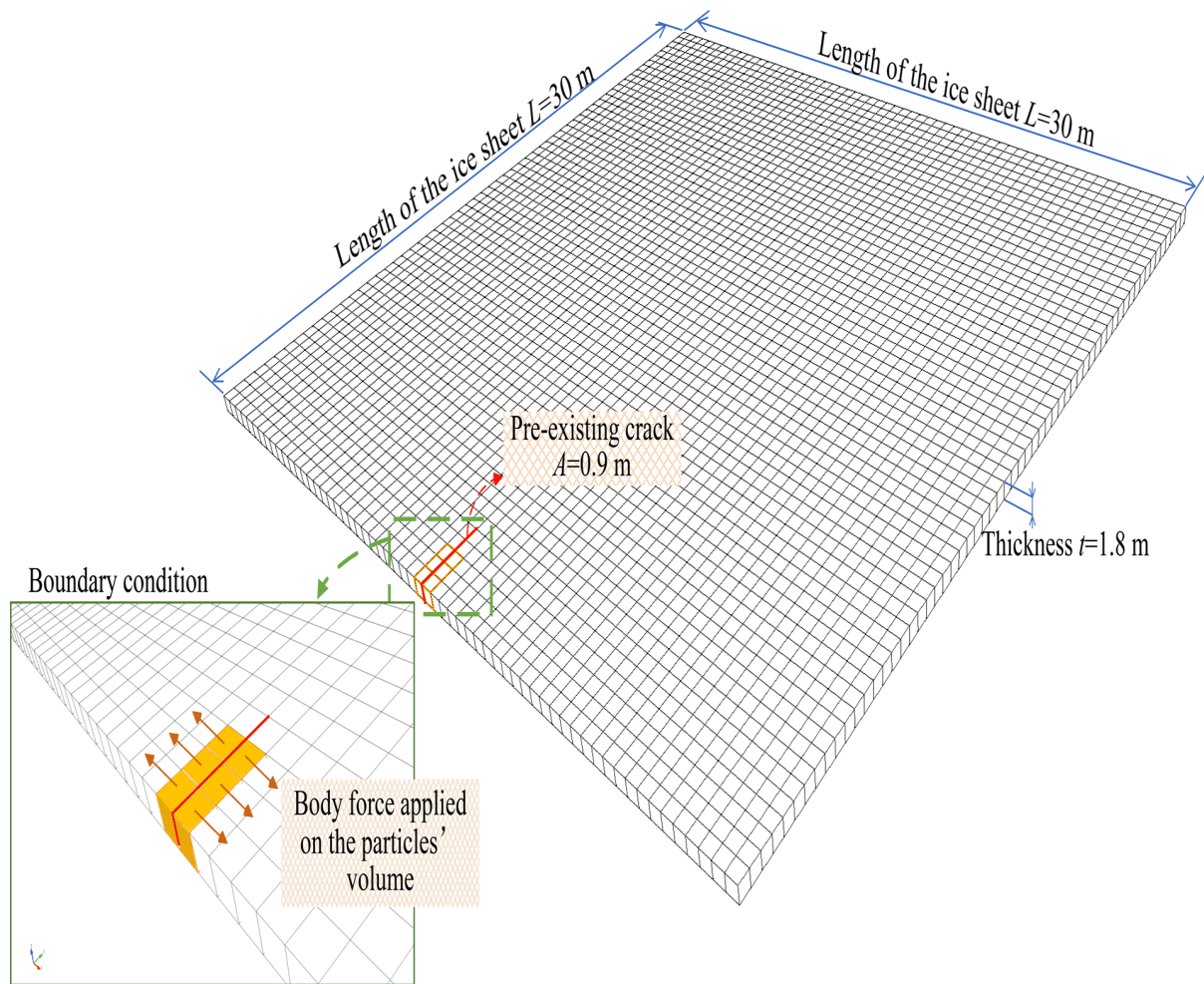**Figure 2.** Failure process and it's mathematical expression in PD theory.

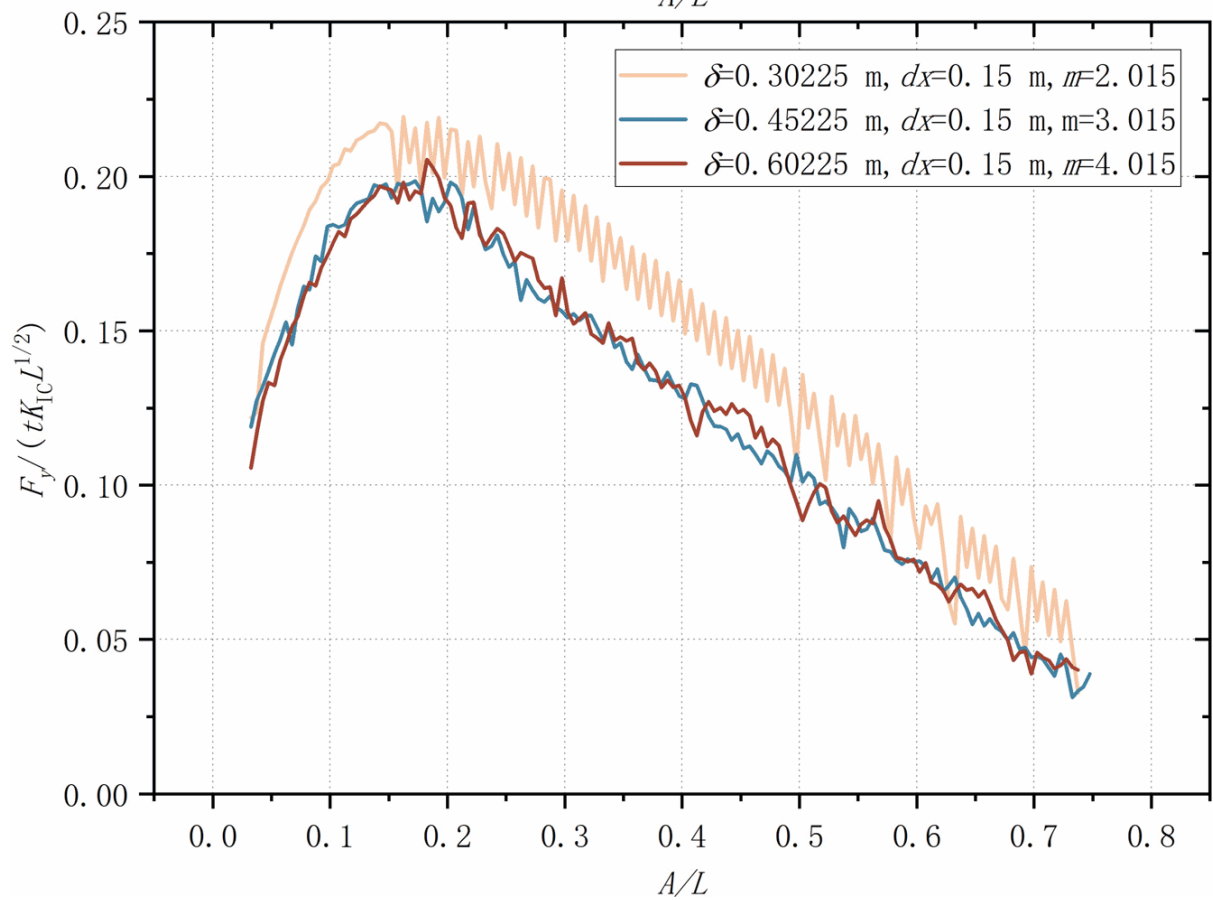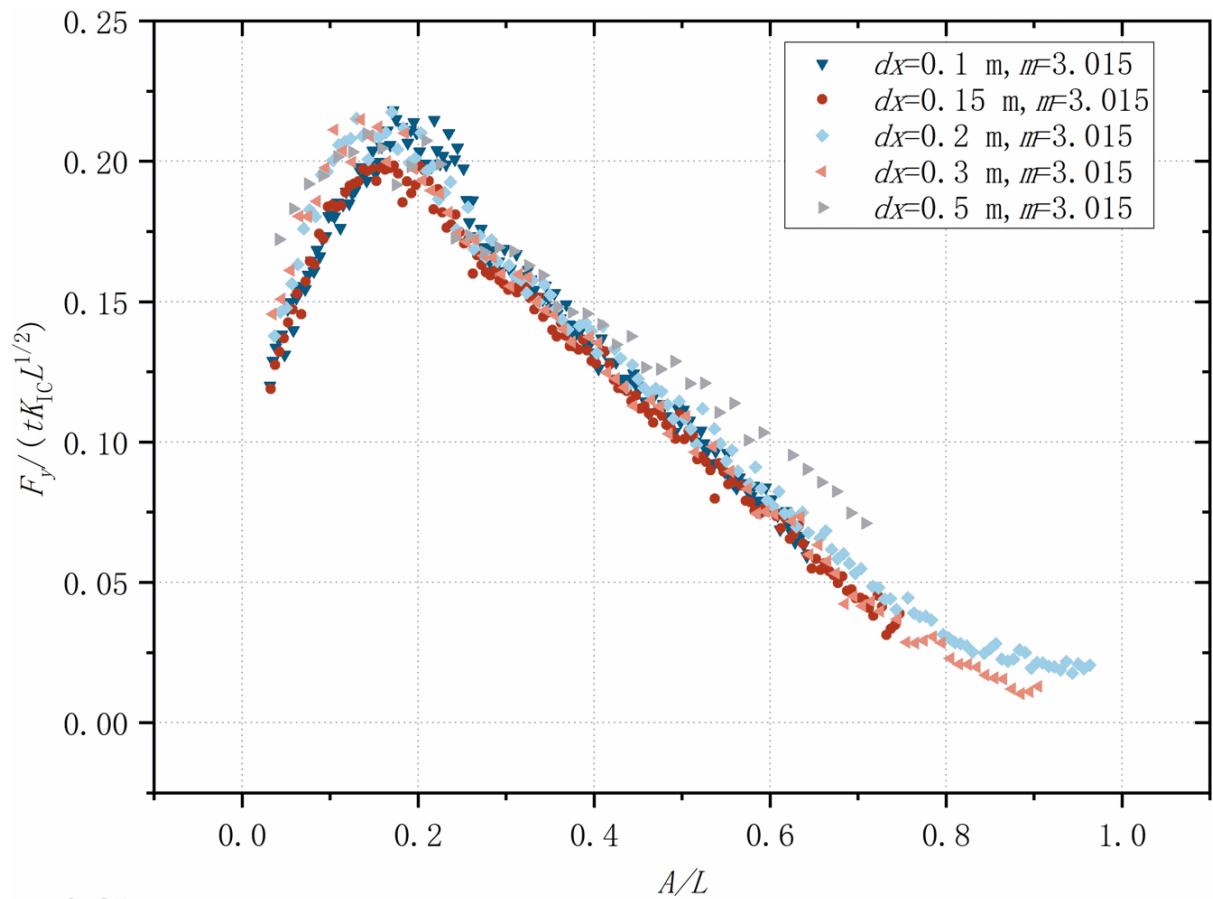**Figure 3.** Model set up for the in-plane splitting of an ECRP.

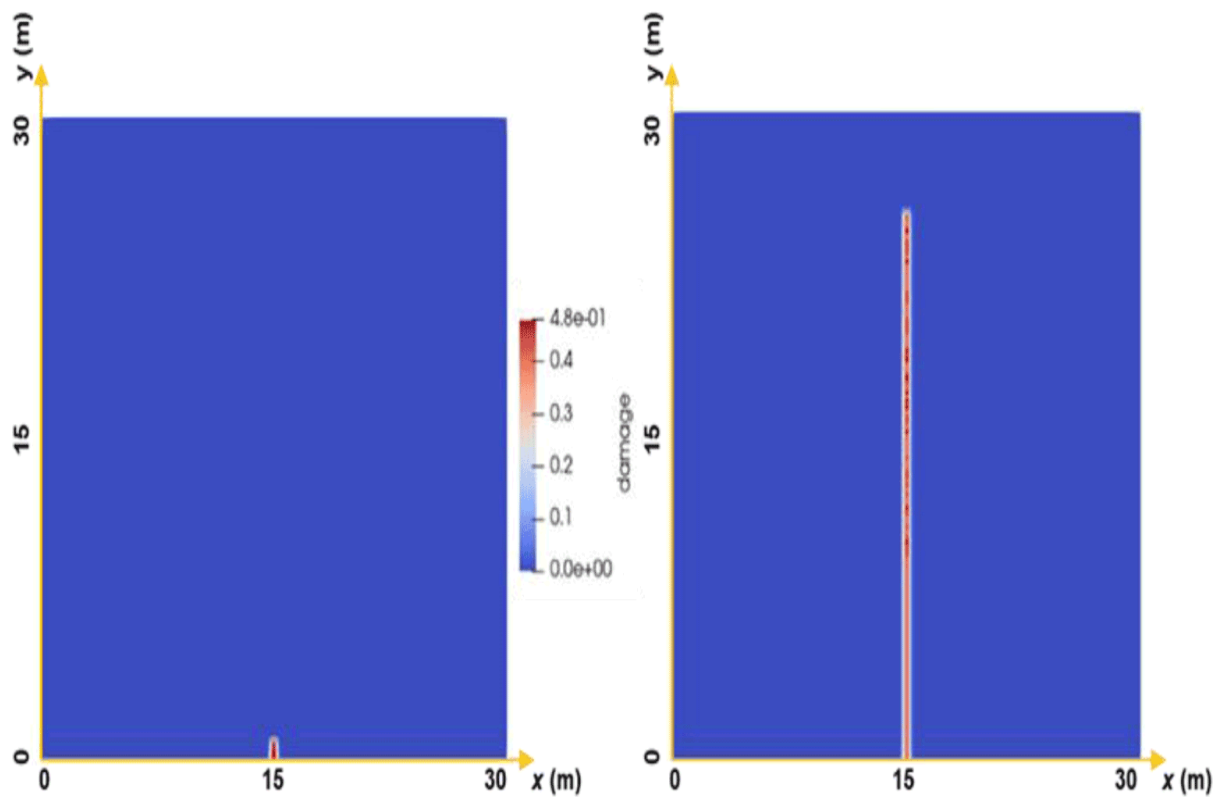https://doi.org/10.1017/aog.2024.43 Published online by Cambridge University Press

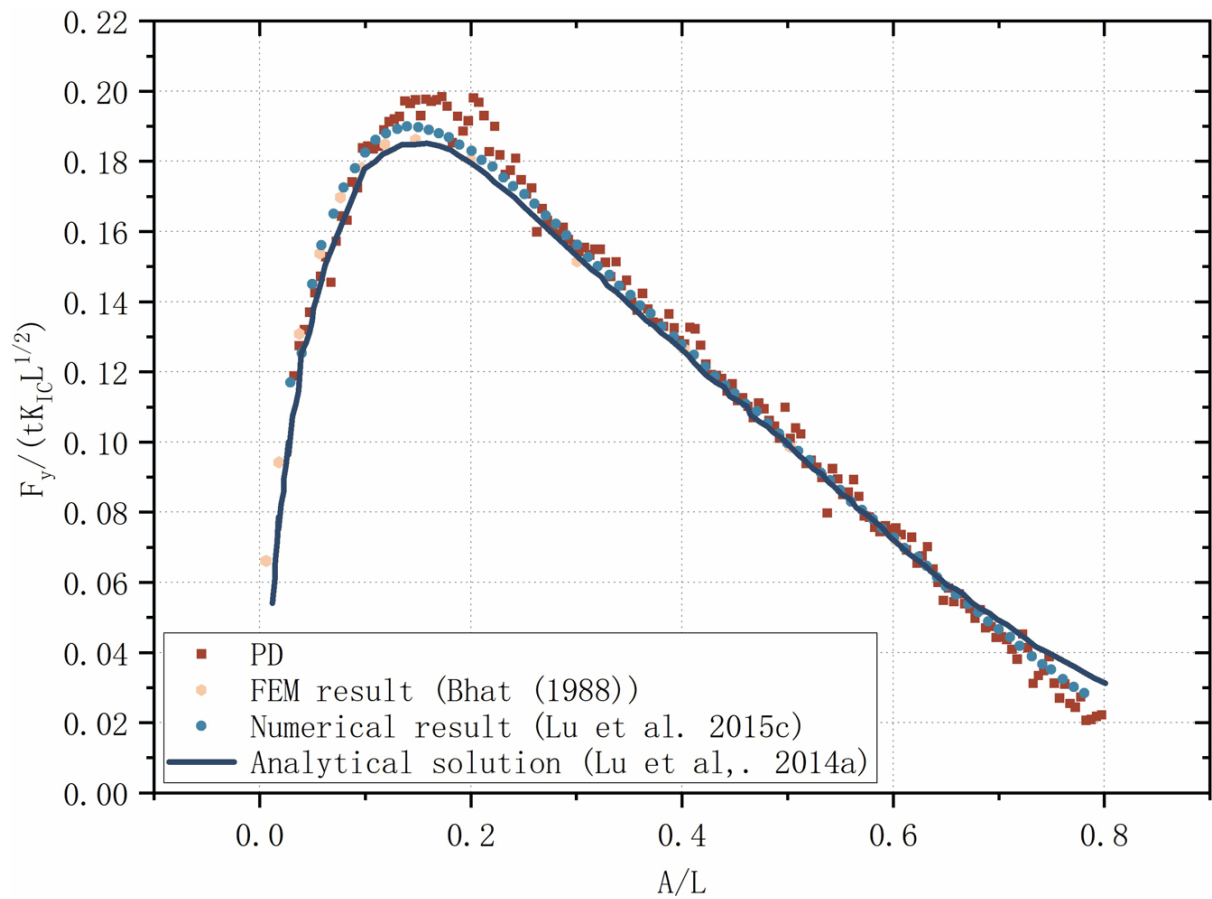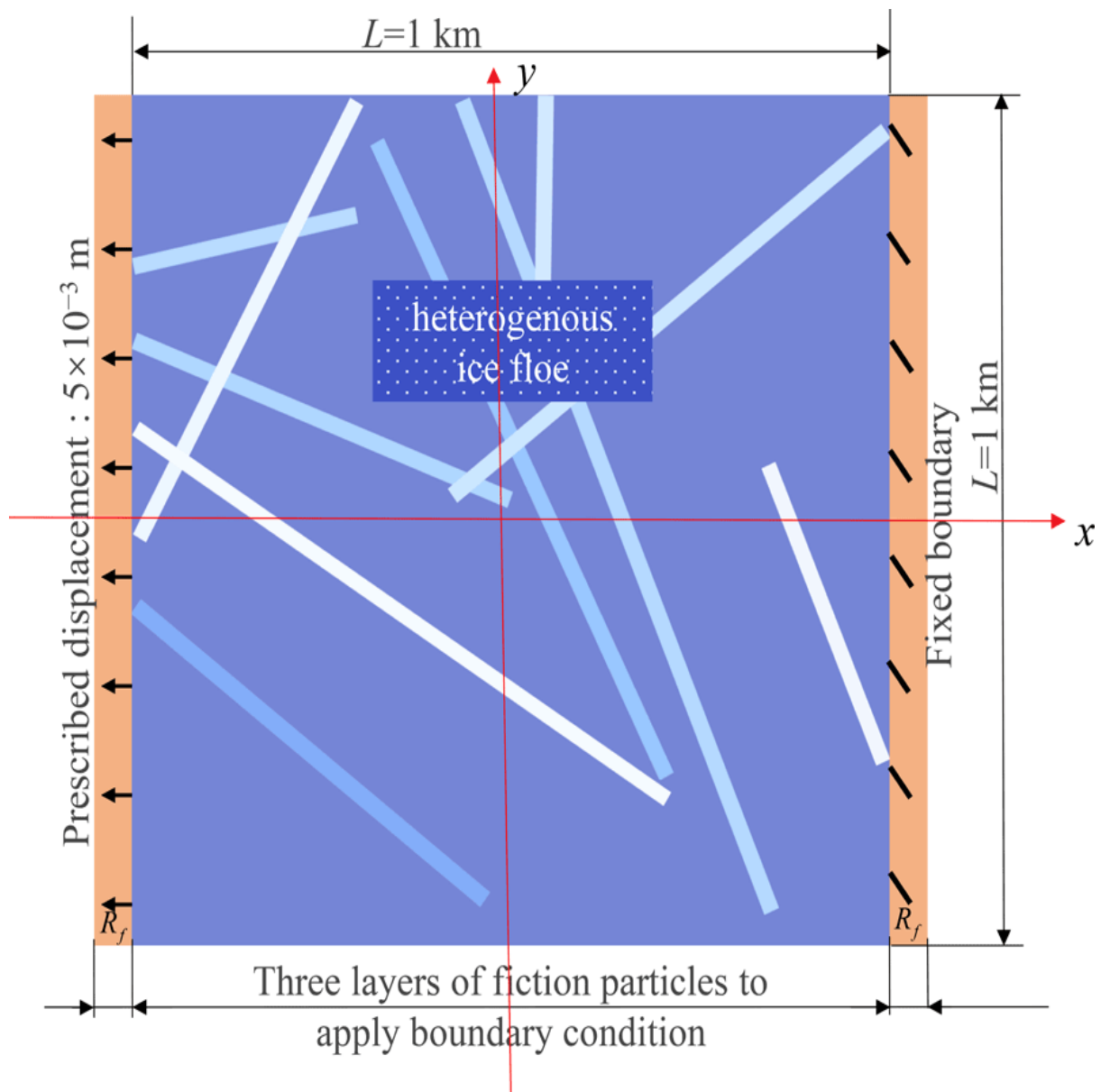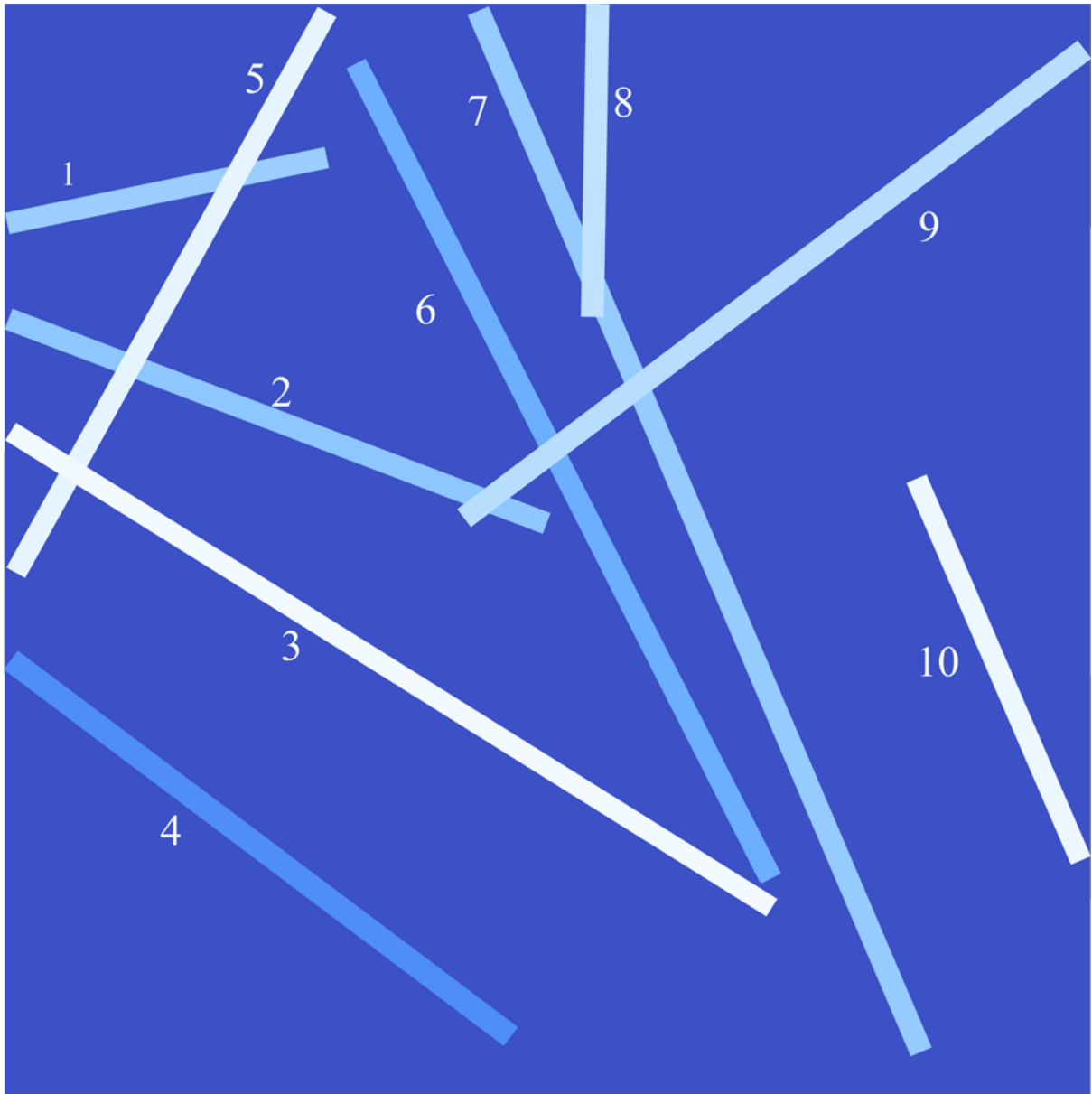**Figure 5.** Crack path of the splitting of an ECRP: initial snapshot (left) and crack propagation snapshot (right).

31

Figure 6. Comparison of the 2D numerical PD scheme with the analytical solution and other numerical methods for the benchmark test: normalized splitting force versus dimensionless crack length.
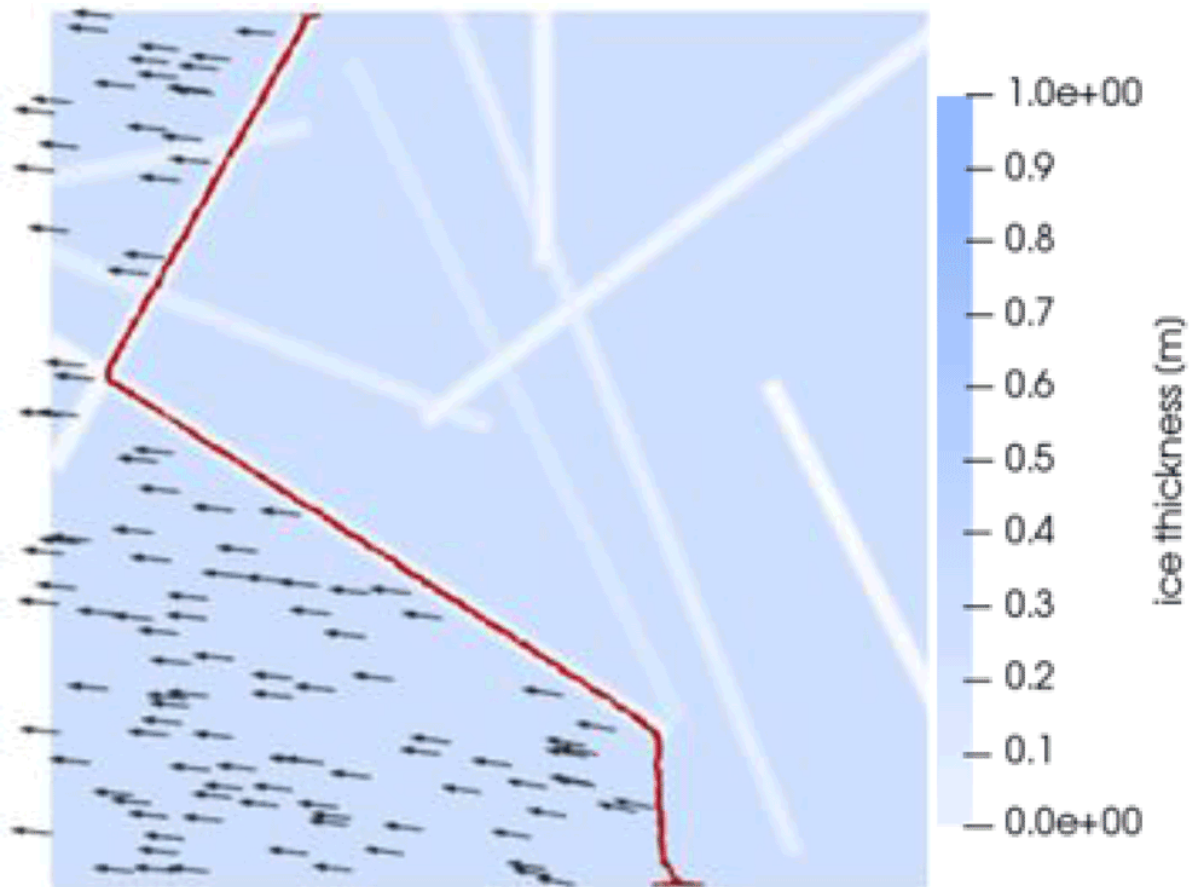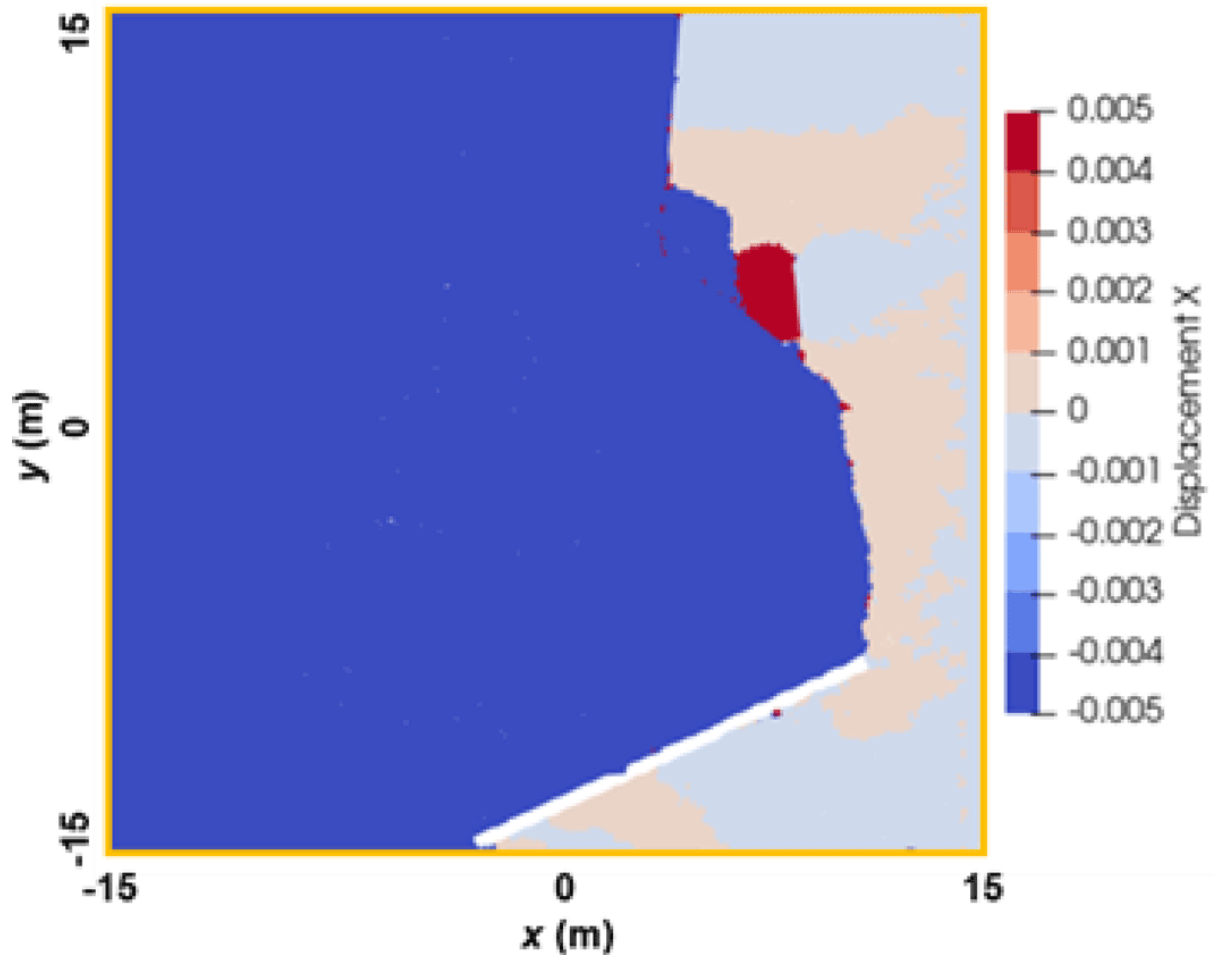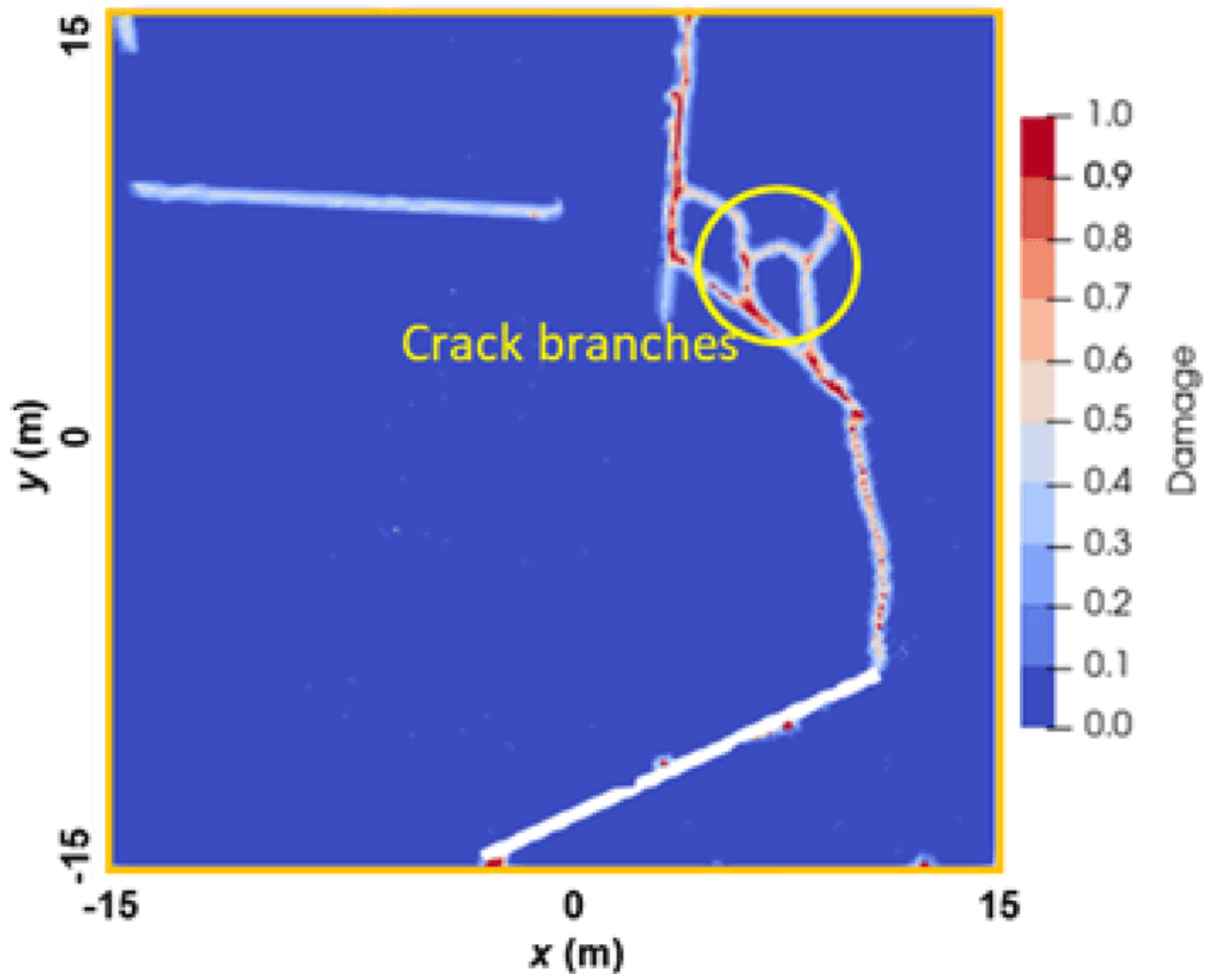
32

34
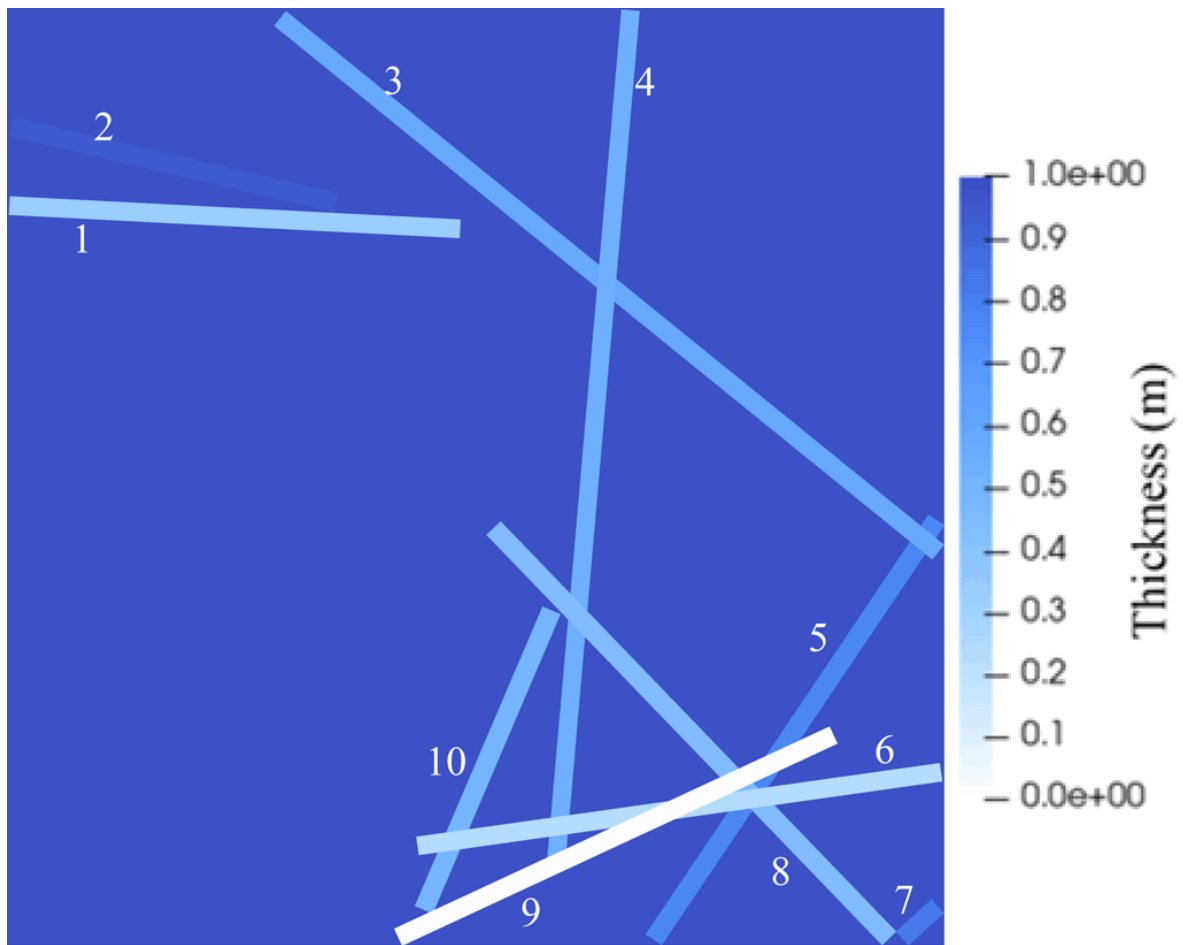
Figure 7. Ice floe model for fracture simulation (Each ice floe has ten different weak zones (#1-10) with different thickness.): (a) illustration of boundary conditions of the heterogenous ice floe fracture; (b) the heterogenous ice floe for case 1; (c) the heterogenous ice floe for case 2.
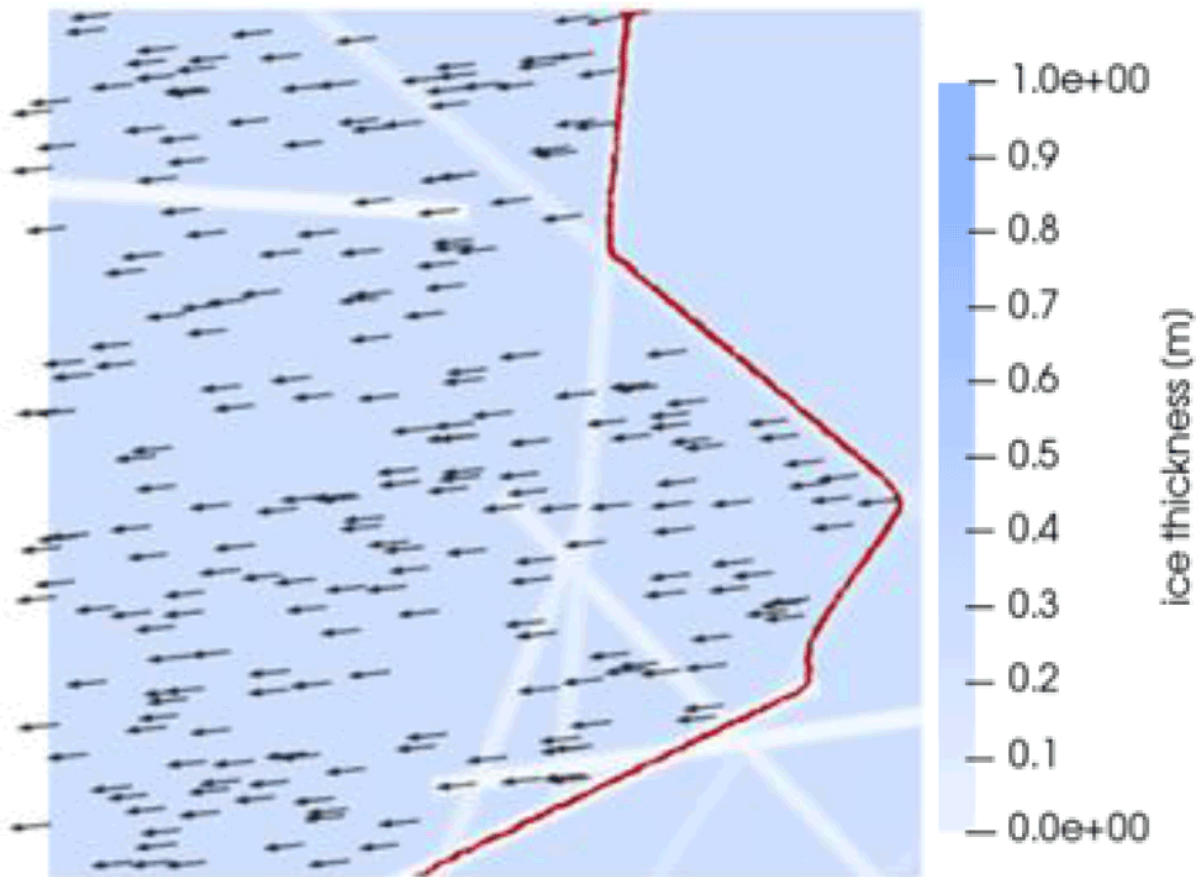
35

37

39

40
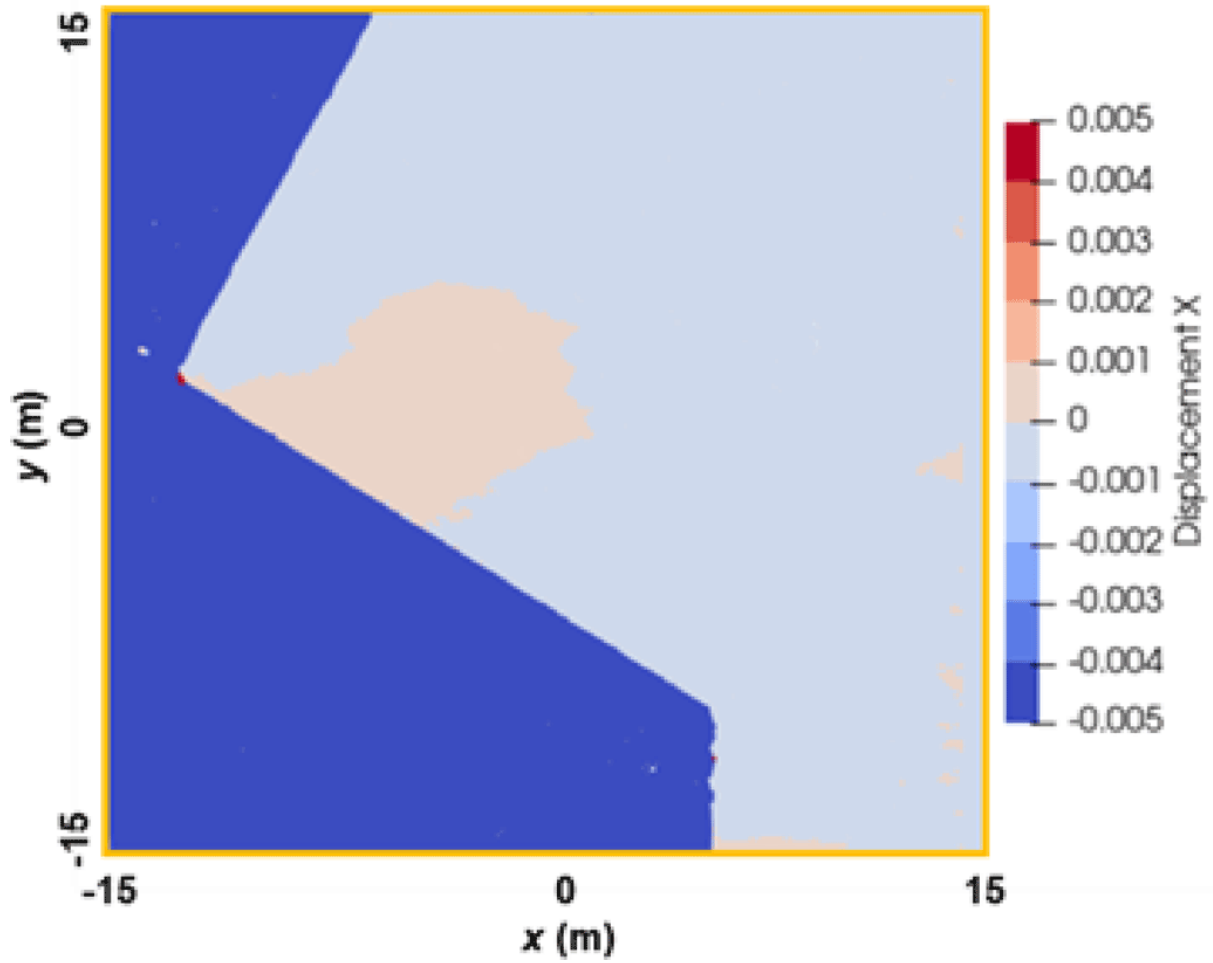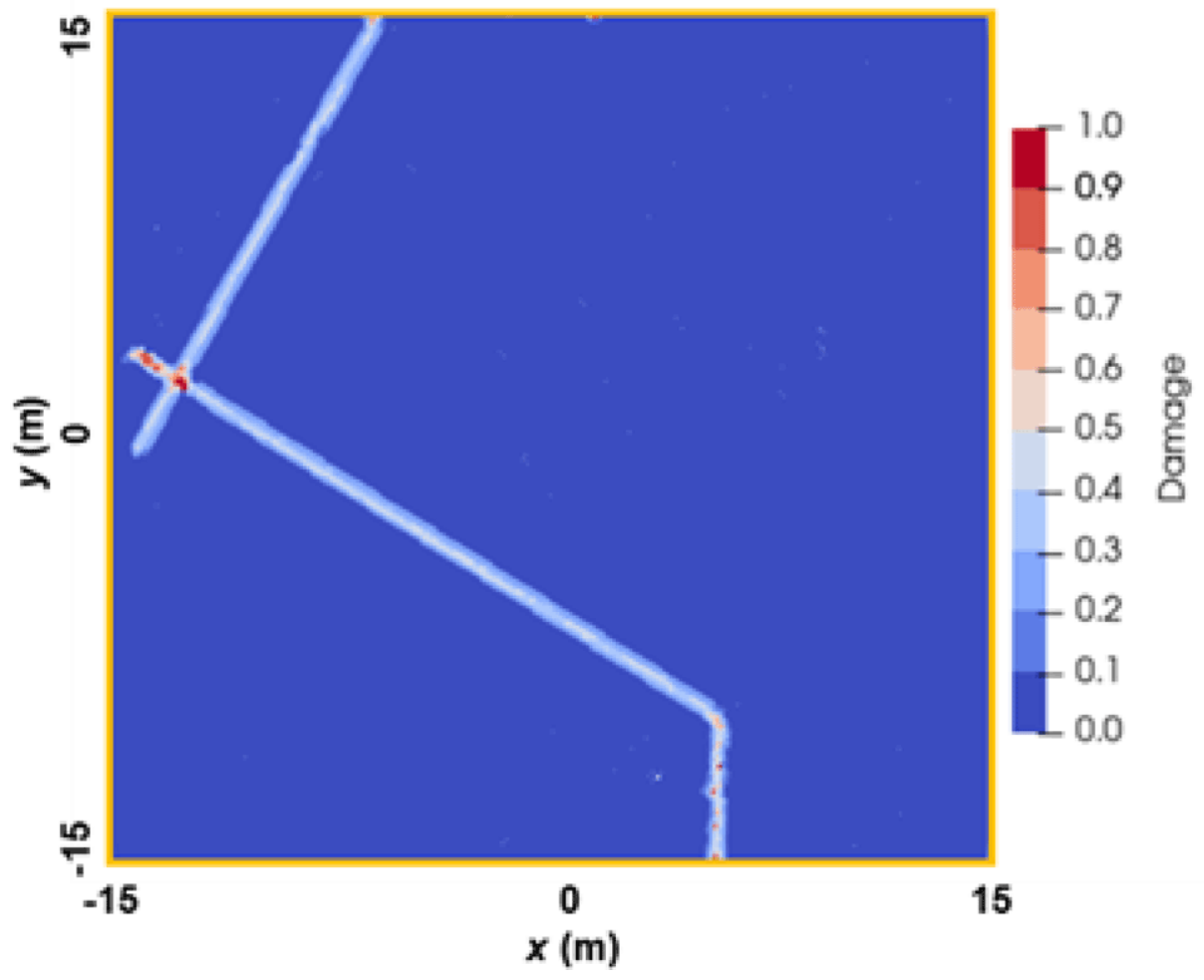
Figure 8. Comparison of the simulation results of the fracture of a heterogeneous ice floe by PD and PFM: (a-1) case 1, PD displacement result, unit [m]; (a-2) case 1, PD damage result, unit [-]; (a-3) case 1, PFM displacement and damage result obtained by Dinh and others (2023) (Black arrows represent the displacement field over the ice floe, while red line indicates crack); (b-1) case 2, PD displacement result; (b-2) case 2, PD damage result; (b-3) case 2, PFM displacement and damage result obtained by Dinh and others (2023) (Black arrows represent the displacement field over the ice floe, while red line indicates crack).
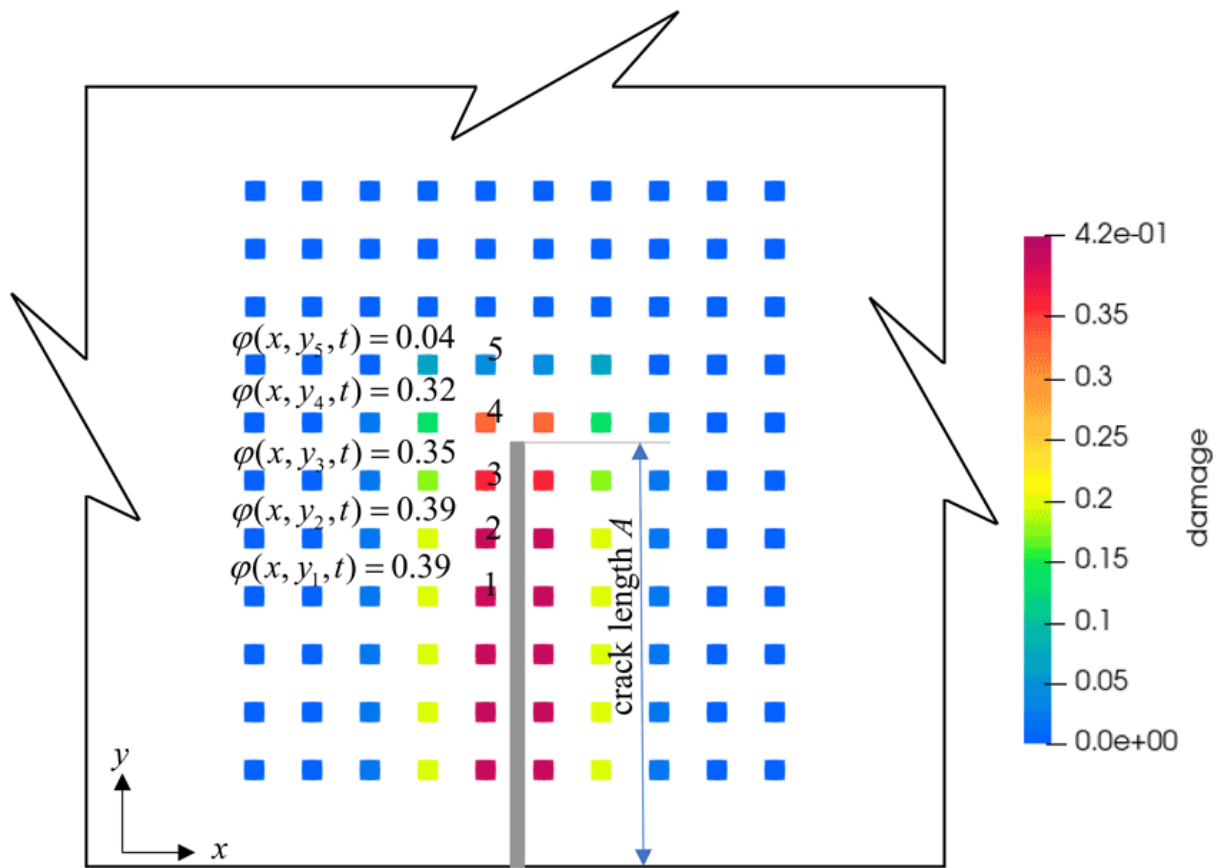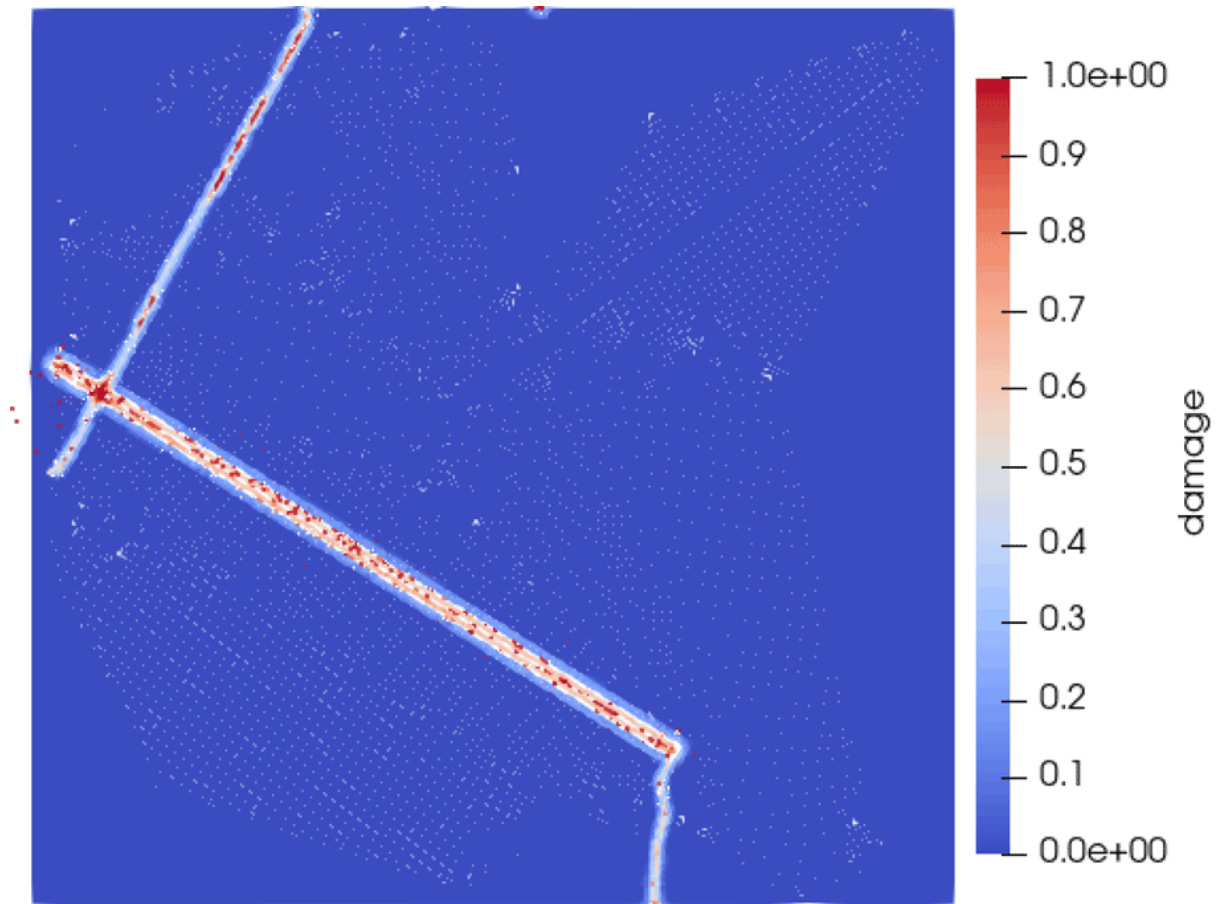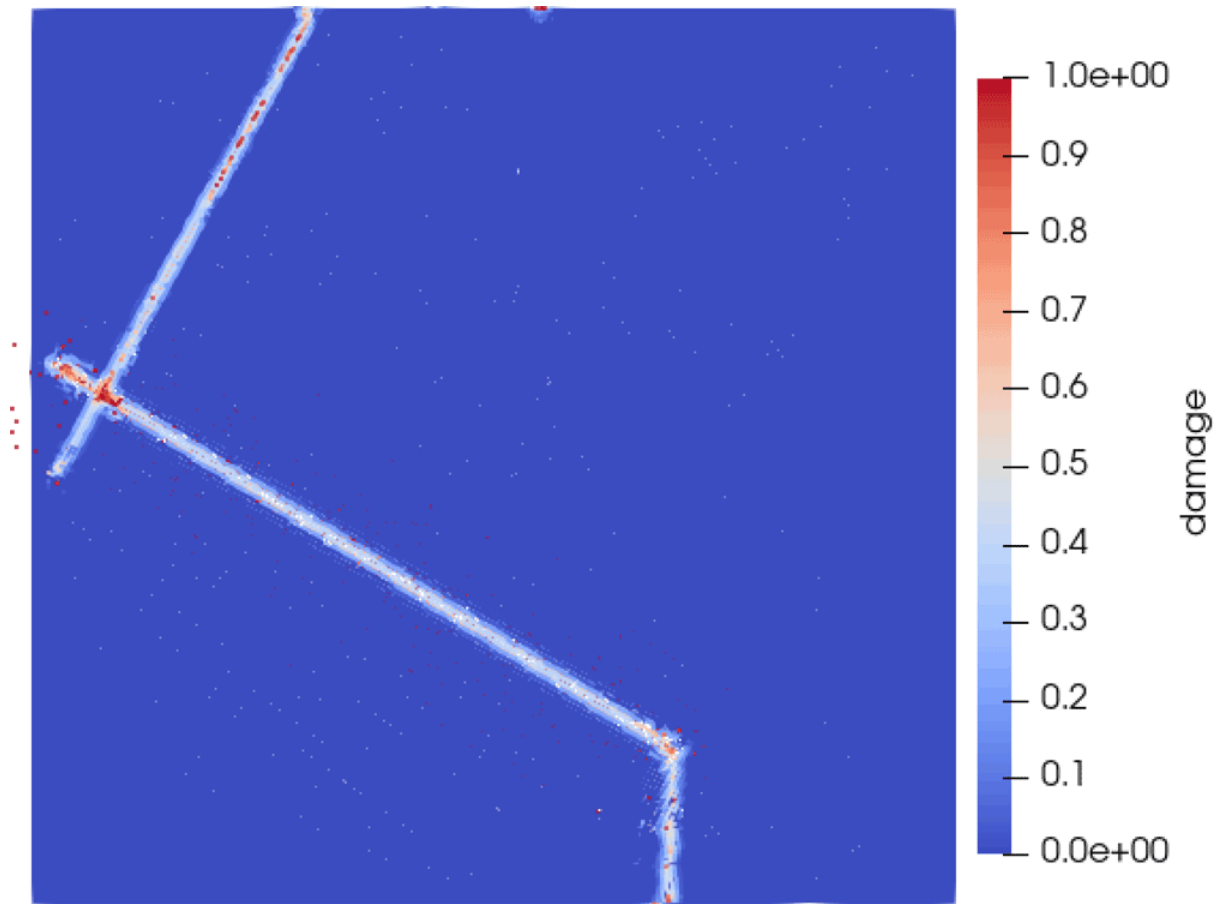
41

Figure 9. Diagram illustrating the definition of crack length.
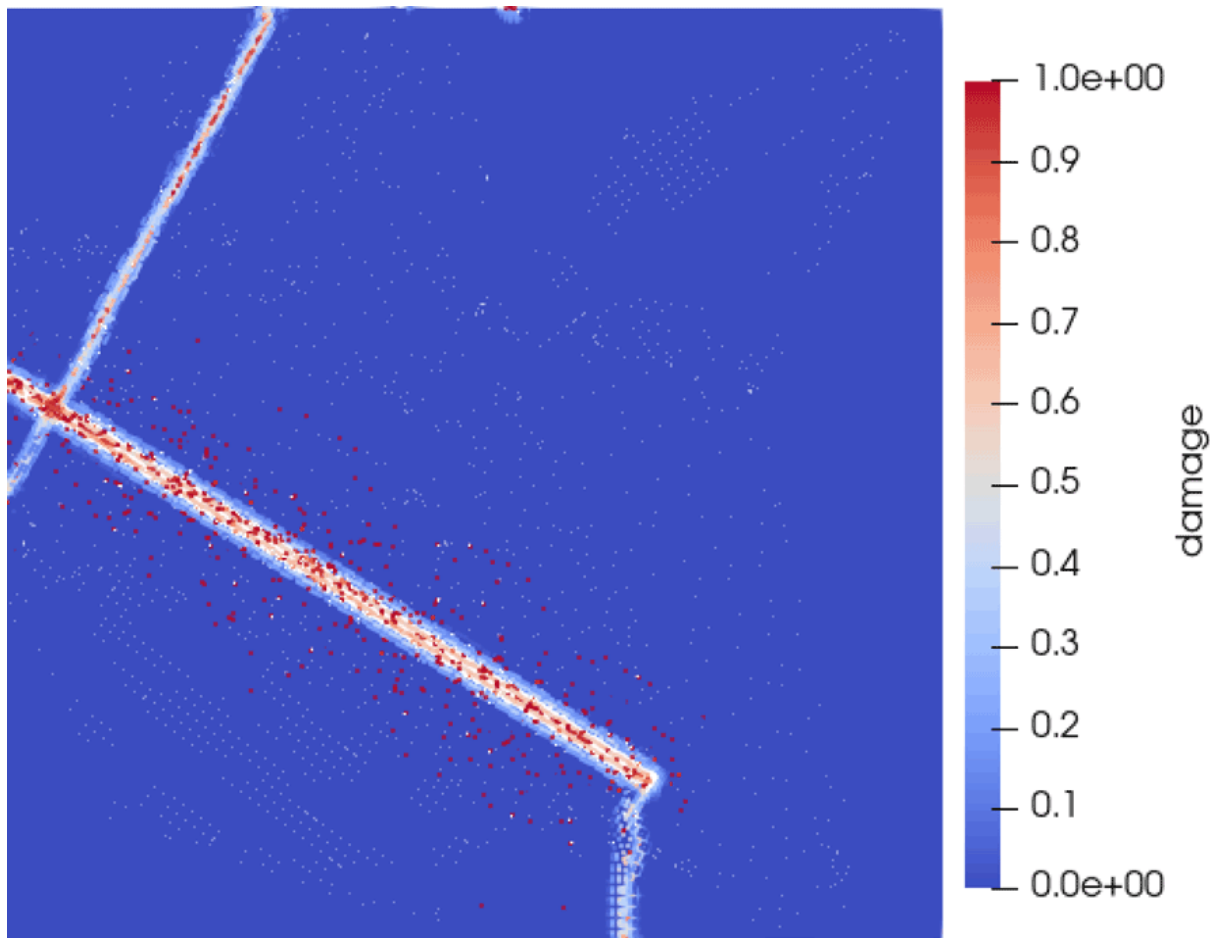
Figure 10. Comparison of the crack propagation between different particle spacings: (a) particle spacing 4 m; (b) particle spacing 5 m; (c) particle spacing 6 m.

List of tables

Table 1. Model setup and calculation information for ECRP.

Geometry of the ice plate L	30 [m]× 30 [m]
Thickness of the ice plate h	1.8 [m]
Elastic modulus E	5 [GPa]
Poisson's ratio v	1/3
Critical energy release rate G_c (Mode-I fracture energy)	15 [N/m]
Ice density ρ	920 [kg/m^3]
Horizon size δ	convergence analysis in Section 3.2

45

Table 2. Information for discretization and the critical stretch in ice tensile failure.

Particle spacing dx	Multiple factor m	Horizon size δ	Critical stretch s_C
0.1 m	3.015	0.3015 m	1.179×10^{-4}
0.15 m	2.015	0.30225 m	1.177×10^{-4}
0.15 m	3.015	0.45225 m	9.176×10^{-5}
0.15 m	4.015	0.60225 m	8.340×10^{-5}
0.2 m	3.015	0.603 m	8.335×10^{-5}
0.3 m	3.015	0.9045 m	6.805×10^{-5}
0.5 m	3.015	1.5075 m	5.271×10^{-5}

Table 3. Input parameters for numerical experiment of heterogenous ice floe fracture.

Geometry of the ice floe L	1 [km] $\times$ 1 [km]
Thickness of the ice plate h	1 [m]
Elastic modulus E	9×10^9 [Pa]
Poisson's ratio υ	1/3
Critical energy release rate G_c (Mode-I Fracture energy)	10 [N/m]
Ice density ρ	920 [kg/m^3]
Particle spacing	4 m, 5 m, 6 m
Critical stretch (corresponding to different particle spacing)	1.134×10^{-5}, 1.014×10^{-5}, 9.261×10^{-6}
multiplier m	3.015

Table 4. Thickness distribution of the two ice floe models.

46

	Case 1			Case 2	
Zone #	Thickness [m]	Width [m]	Zone #	Thickness [m]	Width [m]
1	0.33	20	1	0.17	20
2	0.37	20	2	0.95	20
3	0.01	20	3	0.58	20
4	0.74	20	4	0.53	20
5	0.03	20	5	0.78	20
6	0.54	20	6	0.22	20
7	0.35	20	7	0.84	20
8	0.05	20	8	0.43	20
9	0.21	20	9	0	20
10	0.02	20	10	0.49	20

Table 5. Discretization information for the different particle spacing in fracture of a heterogeneous ice floe.

Particle spacing dx	Numbers of nodes	Horizon size δ	Critical stretch s_C
4 m	64,266	12.06 m	1.134×10^{-5}
5 m	40,976	15.075 m	1.014×10^{-5}
6 m	28,204	18.09 m	9.261×10^{-6}